Electronic Supplementary Material (ESI) for Chemical Communications.

Supporting Information

Spectroscopic Evidence for Origins of Size and Support Effects on Selectivity of Cu Nanoparticle Dehydrogenation Catalysts

Megan E. Witzke,[†,§] Paul J. Dietrich,[‡,§] Malek Y. S. Ibrahim,[†] Kenan Al-Bardan,[†] Mark D. Triezenberg,[†] and David W. Flaherty[†,*]

[†]Department of Chemical and Biomolecular Engineering
University of Illinois Urbana-Champaign, Urbana, IL 61801

[‡]BP Group Research, Naperville, IL 60563

[*]dwflhrty@illinois.edu

[§]These authors contributed equally

Table S1. Catalyst selectivity towards product groups (2.75 kPa C_2H_5OH, 15 kPa H_2, 83.6 kPa He, 503 K, X_{EtOH} = 10%)

Catalyst	**Selectivity** *(%)*						
	Dehydrogenation	**Decarbonylation**	**Dehydration**	**Etherification**	**Esterification**	**Ketonization**	**Aldol**
2 nm Cu-SiO_2	97.3	0	0	0	2.1	$5.18*10^{-3}$	0
8 nm Cu-SiO_2	97.9	0.3	0.14	0.4	1.6	0	0
29 nm Cu-C	97.8	0.3	0	0.2	1.7	0.55	0
35 nm Cu-SiO_2	99.0	0	0	0	0.97	0.1	0
Cu-Al_2O_3	84.0	0.001	0.5	12.5	1.3	0.2	1.5
Cu-ZnO	99.4	0.3	0	0	0.3	0	0
Cu-ZnO-Al_xO_y	97.6	0	0	0	1.9	0.36	0
Cu-Al_xO_y	94.8	0.3	0	0	4.2	0.7	0
Cu-TiO_2	93.0	0	0	0	4.2	0.8	2.3
Cu-MgO	97.7	$1.88*10^{-4}$	0	0	0	0	2.24
Unsupported Cu	99.6	0.17	0	0	0.17	0	0
8 nm Cu-C	98.7	0	0	0	1.2	0.2	0
3 nm Cu-SiO_2	97.2	0	0	0	2.3	0.55	0
30 nm Cu-SiO_2	98.2	0	0	0	1.6	0.4	0
Raney Cu	94.7	0.8	0.1	0	3.2	1.20	0
Cu-CrO_x	98.3	$1*10^{-4}$	0.02	0.1	1.7	0.15	0.05

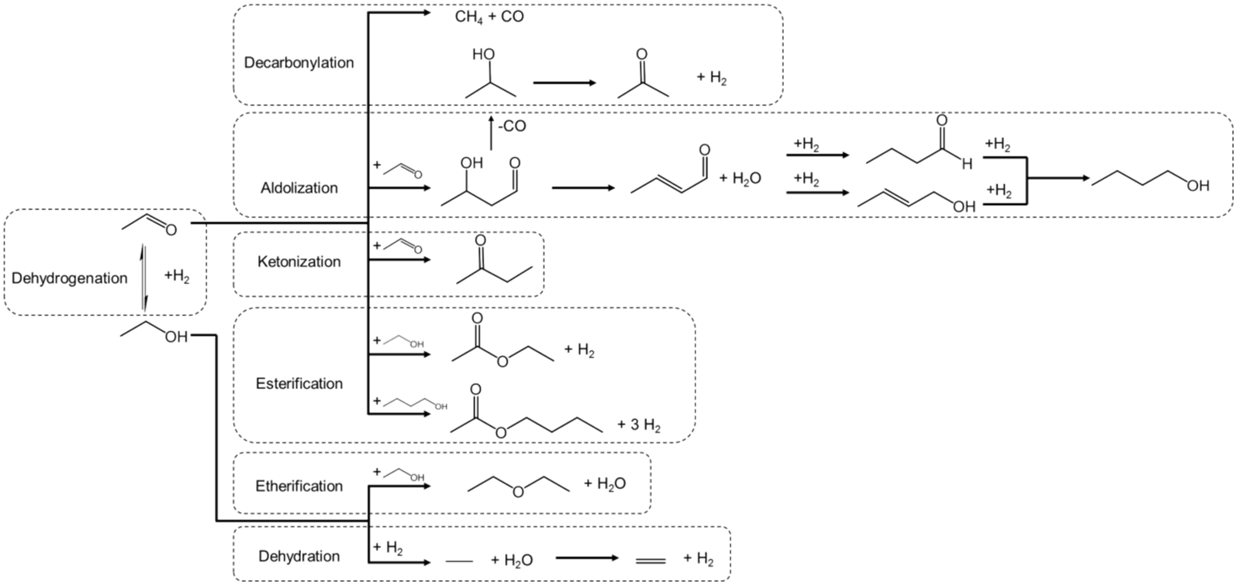

Scheme S1. Products grouped by corresponding reaction pathways described in Table S1

Table S2. Rates of formation of ethyl acetate over Cu-CrO_x at 503 K

Feed Composition	**Residence Time** s * mol Cu_s * (mol oxygenate)$^{-1}$	**Ethyl acetate formation rate** mol $C_4H_8O_2$ * (mol Cu_s s)$^{-1}$
2.75 kPa C_2H_5OH, 15 kPa H_2	8.6	1.4 *10^{-3}
2 kPa C_2H_4O, 6 kPa Toluene	21.2	7.5 * 10^{-5}

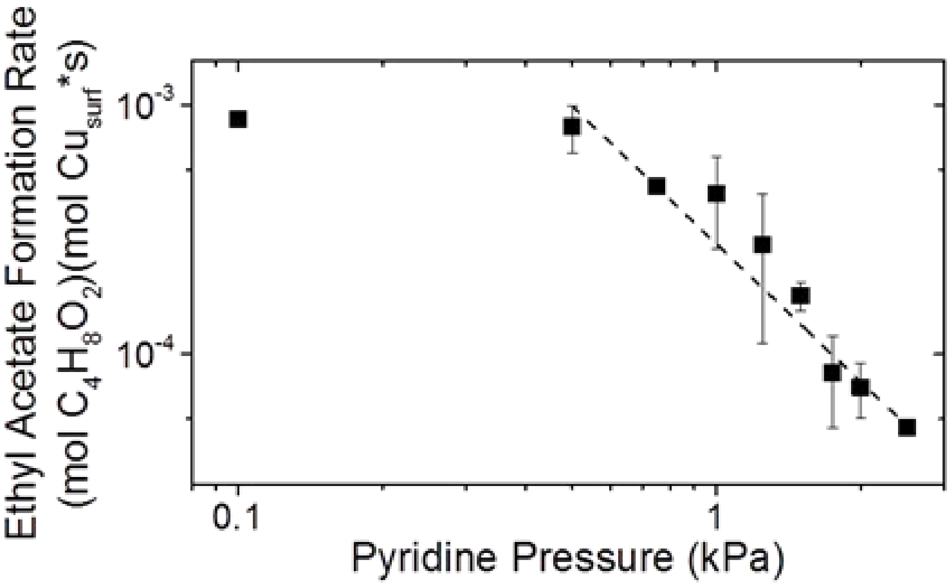

Figure S1. Inhibited rate of $C_4H_8O_2$ formation measured at differential C_2H_5OH and C_2H_4O conversions on Cu-CrO_x (6 nm, ■), at 5 kPa C_2H_5OH, 2.5 kPa C_2H_4O, 16 kPa H_2, bal. He and 503 K. Trend line (dashed) represents power law fit $r_{ester} \sim [\text{pyridine}]^{-1.8 \pm 0.1}$.

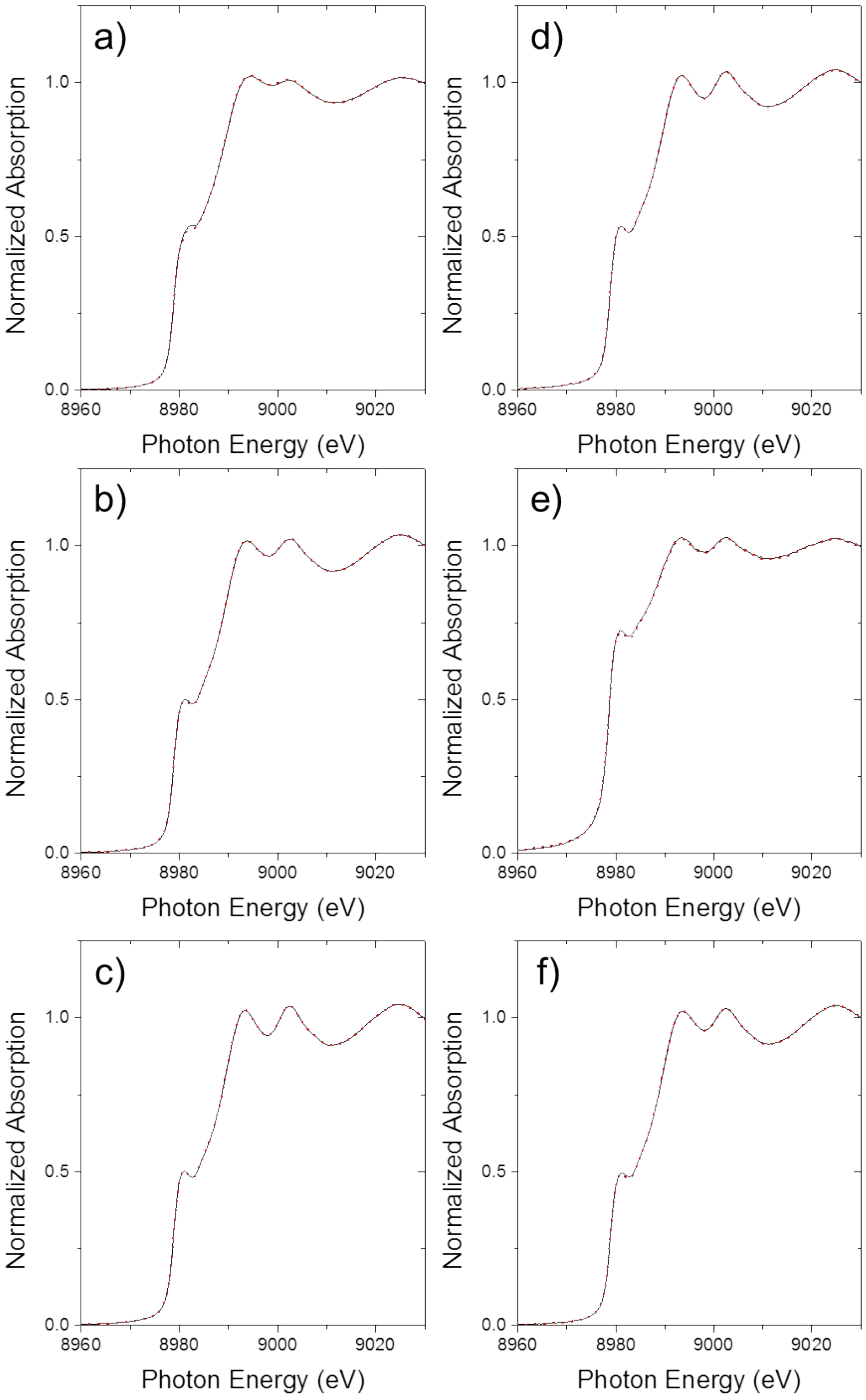

Figure S2. XANES spectra at Cu K-edge for 2 nm Cu-SiO_2 (a), 8 nm Cu-SiO_2 (b), Cu-ZnO (c), Cu-TiO_2 (d), and unsupported Cu (e), and 8 nm Cu-C (f) measured after *in situ* pretreatment (black, solid; 303-573K at 5 K min^{-1} in 40% H_2/60% He, measured at 503 K) and after 30 min at reaction conditions (red, dotted; 4 kPa C_2H_5OH, 0.75 kPa C_2H_4O, 0.25 kPa $C_4H_8O_2$, 30 kPa H_2, 66 kPa He, 503 K).

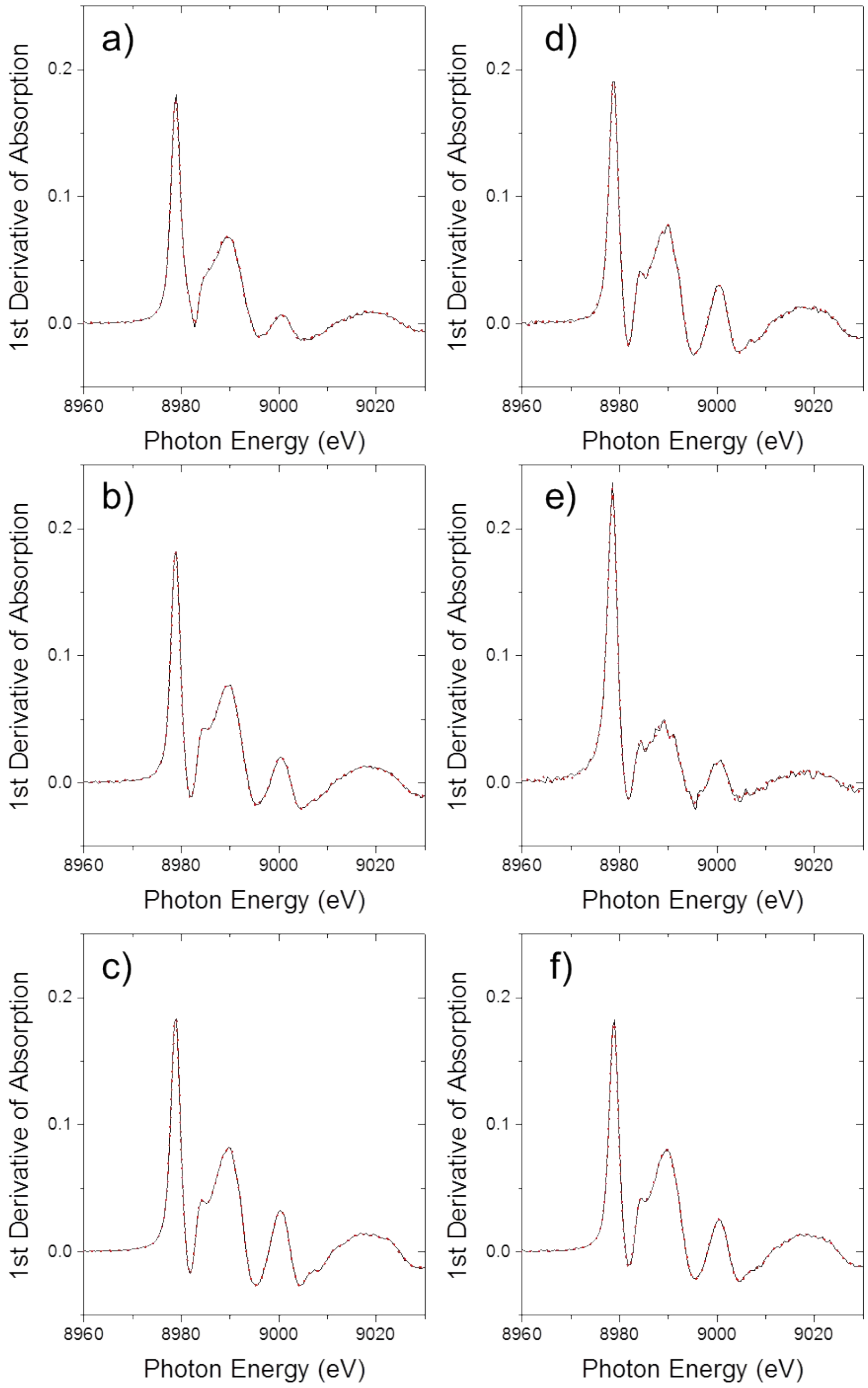

Figure S3. First derivative of XANES spectra at Cu K-edge for 2 nm Cu-SiO_2 (a) 8 nm Cu-SiO_2 (b), Cu-ZnO (c), Cu-TiO_2 (d), and unsupported Cu (e), and 8 nm Cu-C (f) measured after *in situ* pretreatment (black, solid; 303-573K at 5 K min^{-1} in 40% H_2/60% He, measured at 503 K) and after 30 min at reaction conditions (red, dotted; 4 kPa C_2H_5OH, 0.75 kPa C_2H_4O, 0.25 kPa $C_4H_8O_2$, 30 kPa H_2, 66 kPa He, 503 K).

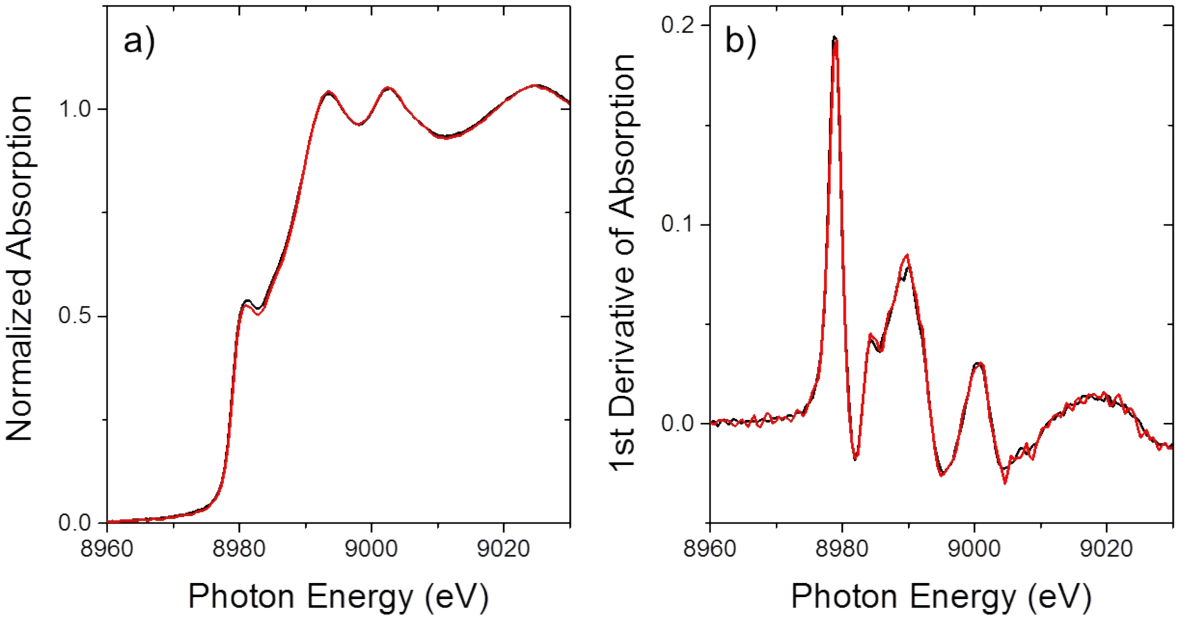

Figure S4. XANES spectra (a) and the 1st derivative of absorption at Cu K-edge for Cu-TiO_2 measured in a tubular plug flow reactor (black) and 6-shooter pellet configuration (red) after in situ pretreatment 303-573K at 5 K min^{-1} in 40% H_2/60% He and measured at 503 K.

Spectra taken over Cu-TiO_2 catalyst in a controlled tubular reactor, which ensures gases and effluent flow over the catalyst, are equivalent to spectra over a self-supporting wafer of Cu-TiO_2 within a 6 sample cylindrical holder; therefore, the XANES of the remaining catalysts measured over self-supporting wafers (Figs. S2 and S3) are assumed to be representative as those done under strict kinetic control.

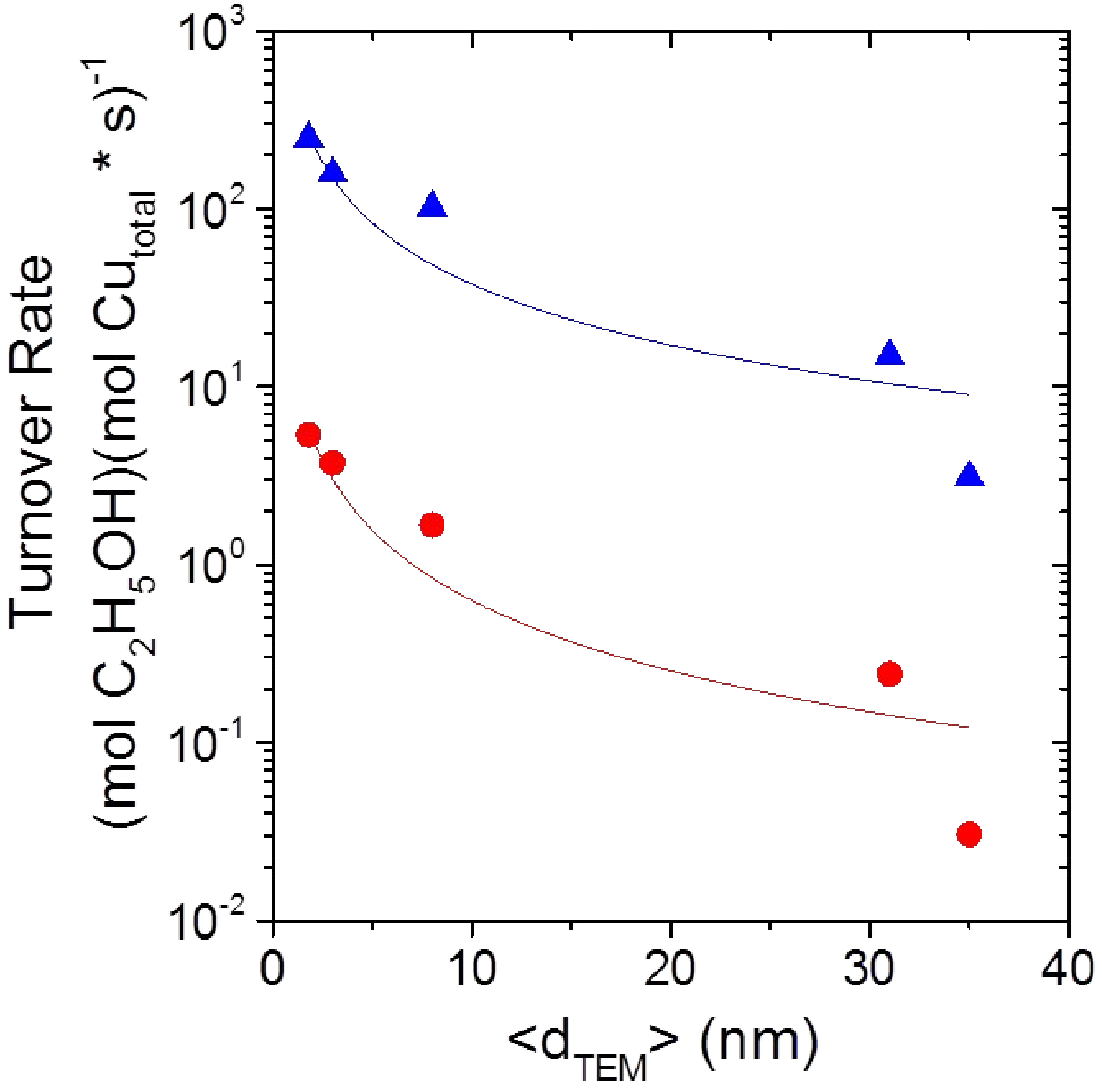

Figure S5. Turnover rates normalized by total mol Cu atoms for esterification (●) and dehydrogenation (▲) on silica supported Cu clusters. Trend lines are power law fits $r_{ester} \sim \langle d_{TEM} \rangle^{-1.3}$ and $r_{dehydro} \sim \langle d_{TEM} \rangle^{-1.1}$.

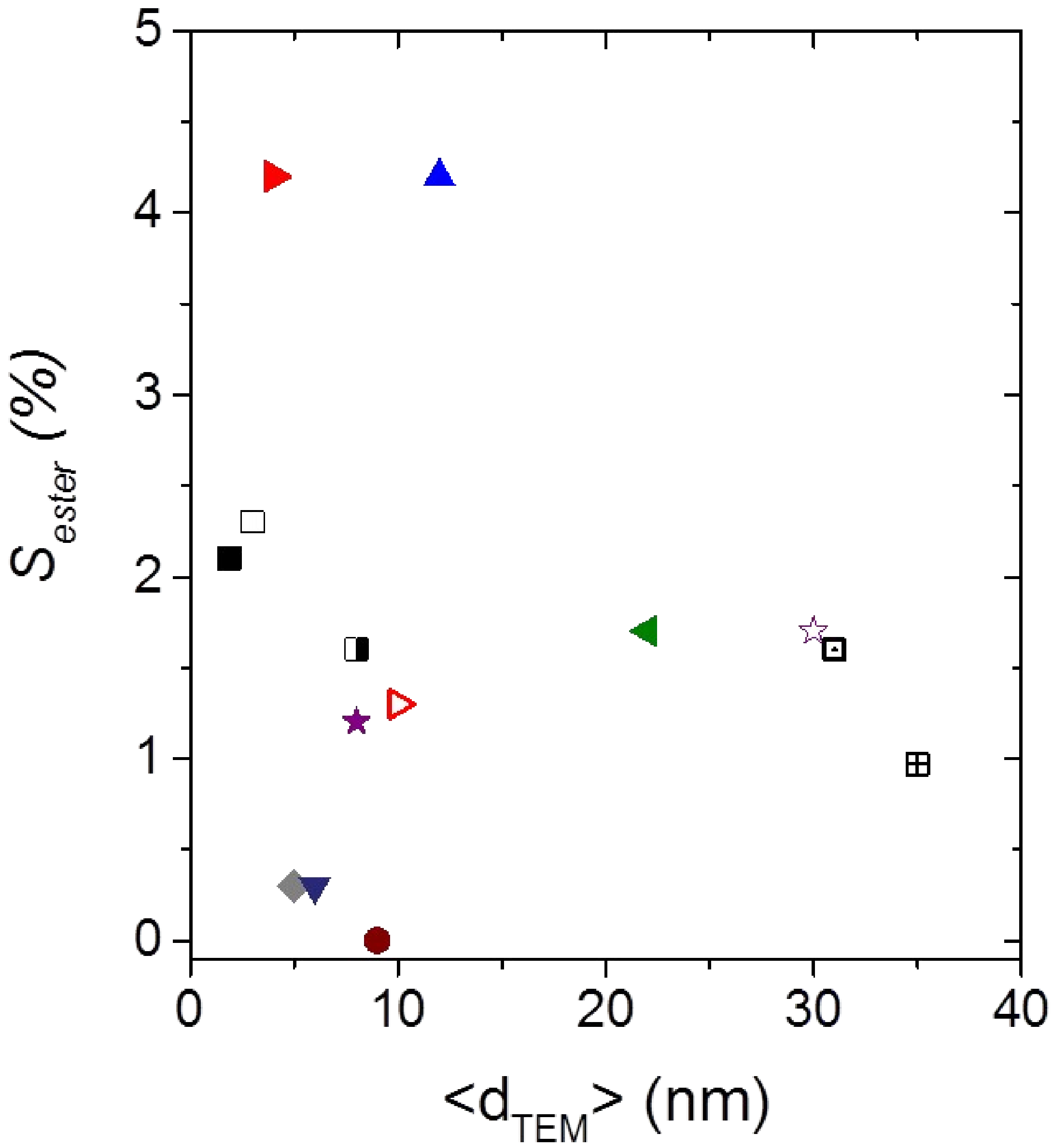

Figure S6. Selectivity towards ethyl acetate formation over Cu clusters of various sizes on supported on ZnO-Al$_x$O$_y$ (5.1 nm, ▼), ZnO (5.4 nm, ◆), TiO$_2$ (7.8 nm, ▲), Al$_x$O$_y$ (3.4 nm, ►), Al$_2$O$_3$ (10 nm, ▷), SiO$_2$ (2 nm, ■; 3 nm, □; 5 nm, ◧; 31 nm, ⊡; 35 nm, ⊞), C (8 nm, ★; 29 nm, ★), MgO (●), CrO$_x$ (6.3 nm, ◄) at X_{EtOH} = 10% (2.75 kPa C_2H_5OH, 15 kPa H_2,83.6 kPa He, 503 K).

Distribution of Cu oxidation states in bulk and surface derivation

Measured bulk oxidation state distribution can be related to surface oxidation state distribution assuming charge transfer occurs only at the cluster–support interface and the clusters have a hemispherical geometry. This means that all the Cu atoms involved in the charge transfer can be estimated using the area of the interface (πr^2), and the total number of Cu atoms can be estimated as the volume ($2/3\ \pi r^3$). The surface atoms from these two regions, which would be responsible for catalyzing reactions, can be estimated as the number of perimeter Cu atoms at the interface, or circumference ($2\pi r$), and the total cluster surface area ($2\pi r^2$). The ratio between the bulk regions and the surface regions proportional to 1/r in both cases, shown in Equation S1:

$$\frac{Interfacial\ Cu\ (\pi r^2)}{Total\ Cu\ \left(\frac{2}{3}\pi r^3\right)} \sim \frac{Perimeter\ Cu\ (2\pi r)}{Total\ surface\ Cu\ (2\pi r^2)} \sim \frac{1}{r} \qquad \text{Eq. S1}$$

Where r is the Cu cluster radius.

Table S3. Esterification rates and selectivities over catalysts and supports synthesized without Cu at equivalent X_{EtOH} = 10% and 503 K and measured surface area

Catalyst	**Contributing Active Sites**	**Feed Composition**			**Esterification Selectivity (%)**	**Ester Formation Rates (mol ethyl acetate * g^{-1} * s^{-1})**	**Surface Area (m^2/g)[a]**
		C_2H_5OH (kPa)	**C_2H_4O (kPa)**	**H_2 (kPa)**			
Cu-TiO_2	Cu-TiO_2	2.75	0	15	4.2	$6.1*10^{-9}$	3.2229
	TiO_2	2.5	0.25	15	14.6	$2.4*10^{-9}$	6.9197
Cu-Al_xO_y	Cu-Al_xO_y	2.75	0	15	4.2	$8.3*10^{-8}$	138.1867
	Al_xO_y	2.5	0.25	15	44.6	$9.1*10^{-9}$	1.1184

[a] Single point surface area measurement from Micromeritics Analytical Services using N_2

The supports synthesized under the same conditions as the corresponding catalysts show significantly different surface area and the esterification rates contributed from the supports cannot be directly subtracted from the Cu catalysts.

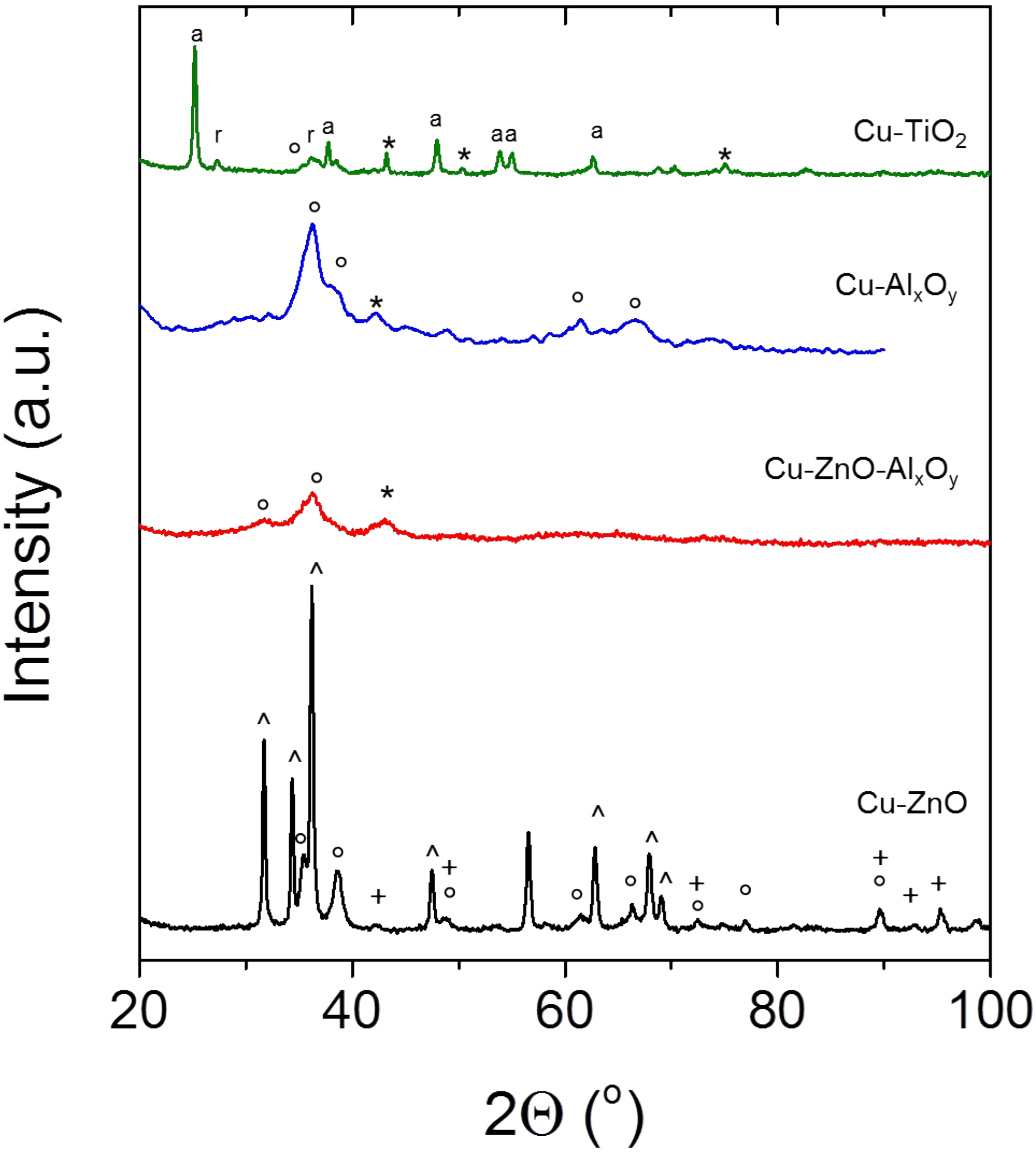

Figure S7. XRD patterns of co-precipitated and sol-gel synthesized catalysts (Cu-TiO$_2$, Cu-Al$_x$O$_y$, Cu-ZnO-Al$_x$O$_y$ and Cu-ZnO) containing phases Cu (*),[1] CuO (°),[1] CuZn alloy (+),[1-3] ZnO (^),[1] and TiO$_2$ anatase (a)[4] and rutile (r)[4] based on previous studies.

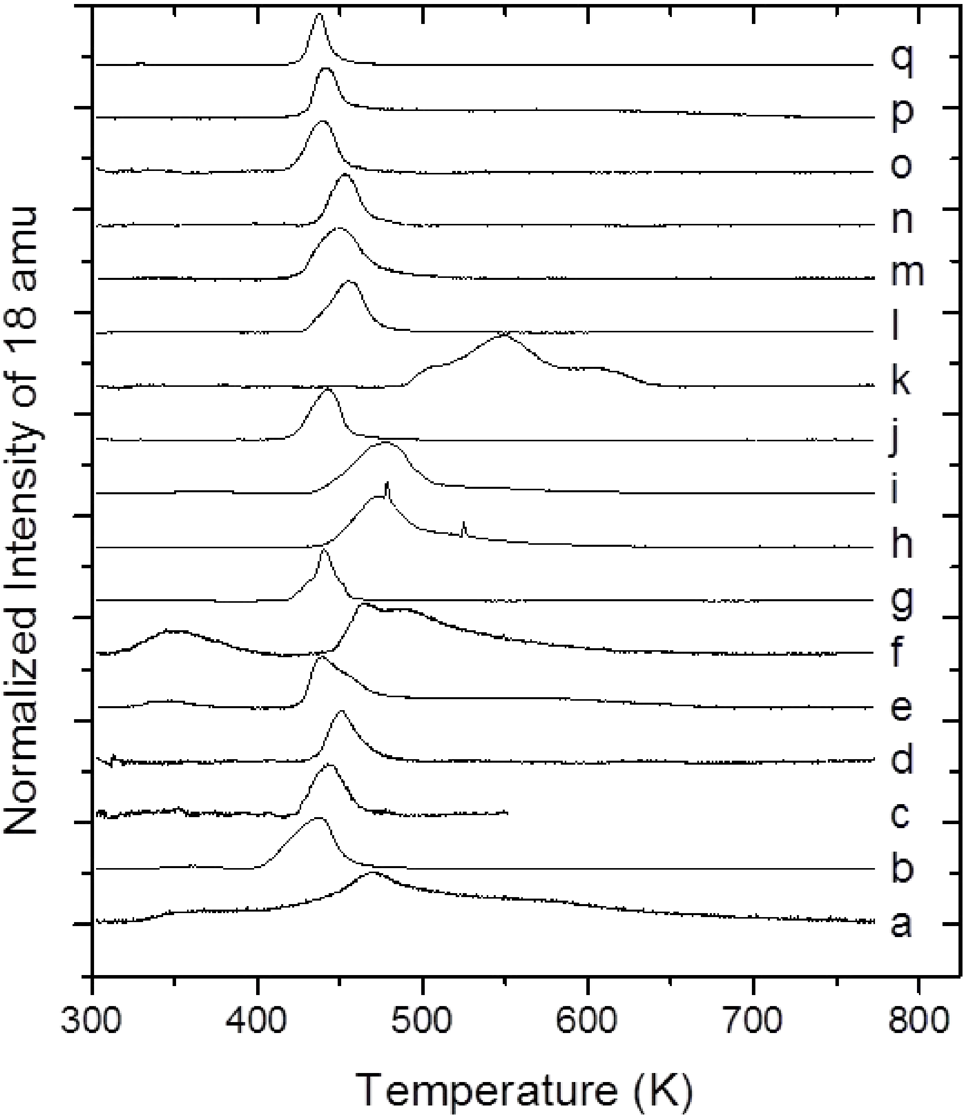

Figure S8. Temperature-programmed reduction profiles in 40% H_2/60% He from 303 K to 773 K at 0.05 K s^{-1} for a) < 1nm Cu-SiO_2, b) 2 nm Cu-SiO_2 , c) 5 nm Cu-SiO_2 , d) 29 nm Cu-C , e) 35 nm Cu-SiO_2, f) Cu-Al_2O_3, g) Cu-ZnO, h) Cu-ZnO-Al_xO_y, i) Cu-Al_xO_y, j) Cu-TiO_2, k) Cu-MgO, l) unsupported Cu, m) 8 nm Cu-C, n) 3 nm Cu-SiO_2, o) 31 nm Cu-SiO_2 p) Cu- CrO_x, q) Raney Cu

SI 2. Catalyst Synthesis, Cluster Size and Composition Catalyst Size, Composition, and Synthesis Conditions

SI 2.1. Catalyst Synthesis

SI 2.1.1. Incipient Wetness Impregnation

Cu-Al_2O_3, Cu-MgO, 8 nm Cu-C, and 31 nm Cu-SiO_2 were prepared by the incipient wetness impregnation (IW) method by impregnating the support Al_2O_3 (Sigma-Aldrich, nanopowder, < 50 nm particle size), activated charcoal (Darco, 20-40 mesh particle size), previously washed and dried MgO (Sigma-Aldrich, 99.995% trace metals basis), or previously washed and dried high surface area silica (Sigma-Aldrich, Davisil Grade 646, 35-60 mesh) with a prepared $Cu(NO_3)_2$ solution. Initially 366.7 mg Cu precursor ($Cu(NO_3) \cdot 2.5H_2O$, Sigma Aldrich ≥ 99.99%) was dissolved in 5 mL deionized (DI) water (Barnstead E-Pure, 17.6MΩ). This $Cu(NO_3)_2$ solution was then added dropwise to the support in 100 μL doses followed by mixing to obtain a homogenous mixture. Impregnation was done until 1.0 mL $Cu(NO_3)_2$ solution was added for every 1000 mg support. The samples were dried in stagnant air at 363 K for > 10 h. The catalysts were calcined at 773 K for 6 h in 300 mL min^{-1} air (Airgas, > 99.999%). Then the catalysts were reduced at 573 K for 6 h in 100 mL min^{-1} H_2 (Airgas, > 99.999%) and 300 ml min^{-1} He (Airgas, > 99.999%).

SI 2.1.2. Ion Exchange

Catalysts 2 nm Cu-SiO_2, 8 nm Cu-SiO_2, 29 nm Cu-C, and 3 nm Cu-SiO_2 were prepared using ion exchange (IE)[5] with varying heat treatments listed in Table 1. Initially, 732.9 mg $Cu(NO_3)_2$ was dissolved in 560 mL deionized (DI) water and 40 mL NH_4OH (Macron Chemicals, 28.0-30.0 % as NH_3) was added to the solution. Previously washed and dried high surface area silica or activated charcoal was added to the Cu solution and allowed to stir > 12 h. Solids were recovered through vacuum filtration over a double layer of filter paper (Whatman, Grade 1, 11 μL pore size), washed with 1 L DI water, and allowed to dry under vacuum for 2 h. Samples were transferred to a glass plate and dried in stagnant air at 363 K for > 10 h before the heat treatments.

SI 2.1.3. Sol-Gel

Cu-SiO_2 (35 nm) was synthesized by the sol-gel method similar to that used by Geravand, *et al.*[6] Initially 146.5 mg $Cu(NO_3)_2$ was dissolved in 100 mL ethanol (C_2H_5OH. Decon Laboratories, 200 proof) followed by the addition of 7.358 mL tetraethyl orthosilicate (Sigma Aldrich, 99.999% trace metal basis). The solution was mixed with a stir bar while heating to 323 K. A citric acid solution (~1M) was prepared by dissolving 42.028 g citric acid monohydrate (Fisher Chemical Certified ACS Granular) in 200 mL DI water. Then 100 mL of the citric acid solution was added to the C_2H_5OH solution and allowed to stir for 2 h while held at 323 K. The resulting gel was dried in stagnant air at 363 K for > 10 h.

Cu-TiO_2 was synthesized by first dissolving 1.464 g $Cu(NO_3) \cdot 2.5\ H_2O$ in 100 mL C_2H_5OH and adding 5.730 g $Ti(OC_3H_7)_4$ (Sigma Aldrich, 98%) while stirring the solution. A precipitate was formed by adding 20 mL of the previously prepared citric acid solution (~1 M). In order to remove the C_2H_5OH, the solution was heated to 323 K for 2 h. The resulting gel was dried in stagnant air at 353 K for > 10 h. The dried catalysts were calcined at 773 K for 6 h in 300 ml min^{-1} air followed by reduction at 573 K for 6 h in 100 mL min^{-1} H_2 and 300 mL min^{-1} He.

SI 2.1.4. Co-precipitation

Catalysts Cu-ZnO, Cu-ZnO-Al_xO_y, and Cu-Al_xO_y were prepared through co-precipitation of Cu with Al and/or Zn. First, a basic aqueous solution was prepared with 2.455 g NaOH (Sigma-Aldrich, ACS reagent, ≥ 97.0 %, pellets) and 3.603 g Na_2CO_3 (Fisher Chemical, Certified ACS Powder) dissolved in 300 mL DI water. An aqueous solution comprised of 100 mL DI water and metal precursors $Cu(NO_3)_2$, $Zn(NO_3)_2 \cdot 6H_2O$ (Sigma-Aldrich, purum p.a., crystallized ≥ 99.0 %); and $Al(NO_3)_3 \cdot 9H_2O$, Sigma-Aldrich, ACS reagent, ≥98%) were prepared separately according to the specific catalyst composition (Table S5). The basic solution (100 mL NaOH/Na_2CO_3) was added to the metal precursor solution with continuous stirring resulting in a precipitate. The combined solution was allowed to stir > 12 h. Vacuum filtration was used to recover the solids, which were subsequently washed with 1 L DI water and dried for 12 h at 363 K in stagnant air followed by oxidative and reductive heat treatments.

SI 2.1.5 Unsupported Cu

Unsupported Cu was synthesized by first preparing $CuCO_3$ from Na_2CO_3 (Fisher, > 99.5%) and $Cu(NO_3)_2 \cdot 2.5\ H_2O$, followed by the decomposition of the $CuCO_3$ in flowing air at 773 K for 6 h. Finally, the sample was cooled to 303 K and reduced at 573 K for 6 h in 100 mL min^{-1} H_2 and 300 mL min^{-1} He.

High surface area Cu (Strem Chemicals, Sponge copper catalyst Raney-type) was pretreated as purchased. A thin layer of Raney Cu slurry was spread in a quartz boat and placed in a horizontal furnace with 300 mL min^{-1} He flow. After drying for 1.75 h, the sample was reduced at 573 K for 6 h in 100 mL min^{-1} H_2 and 300 mL min^{-1} He. Once cooled, the sample was introduced to air for 4 h in 100 mL min^{-1} air and 300 mL min^{-1} He.

Copper chromite (2 CuO Cr_2O_3, Sigma Aldrich) was pretreated as purchased. A sample was calcined at 773 K for 6 h in 300 mL min^{-1} air and reduced to Cu-CrO_x at 573 K for 6 h in 100 mL min^{-1} H_2 and 300 mL min^{-1} He.

SI 2.2 Cluster Dispersion

TEM images were obtained on a JEOL 2010-LaB_6 (200 kV) equipped with a digital camera (Gatan MatScan 1k x1k progressive scan CCD) and taken at ambient temperatures. TEM samples were prepared by grinding approximately 10 mg of sample to a fine powder and dusting onto a holey carbon copper grid (200 mesh, Ted Pella Inc.). The diameters of > 100 clusters were counted from the TEM images obtained, and the surface area normalized average cluster diameter ($<d_{TEM}>$, Table S4) was calculated for each catalyst using:

$$< d_{TEM} > = \frac{\sum_i n_i d_i^{\,3}}{\sum_i n_i d_i^{\,2}} \qquad \text{Eq. S2}$$

where n_i is the number of cluster with diameter, d_i. Figures S9-22 are representative TEM images and cluster size distributions.

X-ray absorption measurements of the Cu K-edge (8980 eV) were conducted on the insertion device beamline of the Materials Research Collaborative Access Team (MRCAT, 10-ID) at the Advanced Photon Source (APS) at Argonne National Laboratory. Ionization chambers were optimized for the maximum current with linear response (ca. 10^{10} photons detected s^{-1}). A third detector in the series simultaneously collected a Cu foil reference spectrum with each measurement for energy calibration. The X-ray beam was 400 mm x 1000 mm, and data was collected in transmission mode. The catalysts were reduced *in situ* in a continuous-flow reactor, which consisted of a quartz tube (1" OD, 12" length) sealed with Kapton windows by two Ultra-Torr fittings. A ball valve, welded to each Ultra-Torr fitting, served as either the gas inlet or outlet. The catalyst was gently pressed into a cylindrical sample holder consisting of 6 wells, forming a self-supporting wafer. The catalyst amount was calculated to give an absorbance (μ_x) of between 2.0 – 2.5, and an edge step ($\Delta\mu_x$) of at least 0.2. All spectra were collected in quick scan mode. A reduced scan range ($-100 < E_0 < +400$ eV, ~30s/scan) was used for the in situ TPR experiments described in Section SI 1.3. Full spectra (-200 eV $< E_0 <$ 1000 eV) to capture the EXAFS were taken at 303 K in flowing He before and after temperature programmed reduction treatments described in Section SI 2.3.

Data analysis was performed using the Demeter (Athena and Artemis) XAS Data Processing software package and standard data processing methods.[7] Spectra were first normalized by fitting the pre- and post-edge regions to linear and cubic polynomials. The XANES were isolated by inspecting the normalized spectra in a range of -20 eV $< E_0 <$ 80 eV. For in situ TPR fitting, the XANES were fit with a combination of the following references: bulk oxides CuO, Cu_2O; small particle supported CuO and Cu_2O; and Cu foil. Fitting was performed with the linear combination XANES fitting function in Athena. EXAFS spectra were isolated by removing the background using piecewise splines to fit a background function to the data. The k-space EXAFS data was k^2-weighted, and Fourier transformed to produce the R-space plots. Data was then fit in R-space using the quick first shell approximation to fit the first coordination sphere (data between 1 and 3 Å) to extract coordination numbers and bond distances. Particle sizes were estimated from the EXAFS coordination numbers using the correlation derived by Miller et al.[8]

SI 2.3. Composition and Structure

Powder X-Ray Diffraction using a Siemens/Bruker D-5000 (Cu K-α, 0.15418 nm) was used to determine crystallographic structures of catalysts and supports (Fig. S7). Approximately 300 mg of samples were finely ground to < 200 mesh using a mortar and pestle before being scanned at a rate of 0.0167° s^{-1} with 0.1° resolution at 40 kV and 30 mA. Metal weight loadings were measured using Inductivity Coupled Plasma-Optical Emission Spectrometry (ICP-OES) and CHN analysis, shown in Tables S4 and S5.

Temperature programmed reduction (TPR) experiments were performed in duplicate with online mass spectrometry (TPR-MS) and X-ray Absorption Near Edge Spectroscopy (TPR-XANES) in order to determine oxidation state of catalysts at various pretreatment temperatures. Catalyst samples and silicon dioxide (Sigma Aldrich, analytical reagent) with total mass of 500 mg were loaded in a packed bed reactor comprised of a quartz tube with frit (12 mm OD) in a down flow orientation. Reactor temperature was regulated by an electrically heated furnace (Lindberg, 55035-A), an electronic temperature controller (Watlow, EZ-Zone), and a K-type thermocouple contained in a 1/16" stainless steel sheath (Omega, TJ36-CASS-116U-18- -SMPW-M). TPR-

MS measurements were taken after an oxidative treatment in flowing air (14 mL min^{-1}, purified using a zero air generator (Parker, 76-830)) heated from 303 K – 473 K at a rate of 5 K min^{-1} and held at 473 K for 2 h. The sample was then cooled to 303 K in flowing He (25 mL min^{-1}), after which reduction was performed in 40% H_2/He to 773 K at 5 K min^{-1} and held at 773 K for 1 h. Gas flow rates were regulated with digital mass flow controllers (Parker Porter, Model 601) and a digital controller (Parker Porter, CM-400). Composition of exit gases were measured with a quadrupole mass spectrometer (QMS, Pffeifer Vacuum Thermostar D-35614) monitoring masses 2, 4, and 18 amu and reduction profiles are shown in Figure S8.

TPR-XANES experiments were performed at the MRCAT 10-ID beamline described in Section SI 1.2. After an oxidative treatment at 573 K in stagnant air for 2 h, the reactor was cooled to 303 K in flowing He. Initial full scans were taken before beginning the temperature programmed reduction. The *in situ* TPR was performed under flowing 40% H_2/He (100 ml min^{-1}) at 5 K min^{-1} to 773 K (measured by an internal thermocouple at the position of the samples). XAS data was taken continuously with a scan resolution of ~30 s as described in 2.2. XANES data was then processed according to the procedures in Section SI 2.2 and fit using linear combinations of the references described in Section SI 2.2.

SI 2.4 Catalyst Selectivity and Activity

Rate and selectivity measurements were conducted in a packed bed reactor comprised of borosilicate tube (12 mm OD) at atmospheric pressure (101 kPa). The reactor was heated with a three-zone electrically heated furnace (Applied Test Systems, 3210) that was controlled by an electronic temperature controller (Watlow, EZ-Zone). The catalyst temperature was measured by a K-type thermocouple contained within a 1/16" stainless steel sheath (Omega, TJ36-CASS-116U-18- -SMPW-M) with the tip inserted in a nipple at the catalyst bed. Silicon dioxide (SiO_2, Sigma-Aldrich, washed and calcined, analytical grade) was used as a diluent to keep the bed volume constant at 0.25 mL. The pressure drop across the reactor was measured using a pressure gauge (Matheson) upstream of the reactor and was kept < 10 kPa.

Catalysts were pretreated *in situ* by heating to 573 K at 5 K min^{-1} and holding for 1 h in flowing 40% H_2 (Airgas, 99.999%) / He (Airgas, 99.999%) at 265 mL min^{-1} prior to all catalytic measurements, unless otherwise stated. Gas flow rates (H_2 and He) were controlled using mass flow controllers (Parker Porter, Model 601) coupled to a digital controller (Parker Porter, CM-400). Ethanol (C_2H_5OH) and acetaldehyde (C_2H_4O) were fed to the system with syringes (Hamilton Reno, Nevada 5 mL) connected to an automated pump (KD scientific, Legato 110) that controlled their flow rates. Transfer lines at the liquid inlet and downstream were heated to above 373 K monitored with K-type thermocouples (Omega, 5TC-GG-20-72) displayed on a digital reader (Omega, 402B-TC) to avoid condensation of reactants and products.

An on-line gas chromatograph (Agilent, HP 6890) equipped with a capillary column (HP Plot Q, 30 m length, 0.320 mm inner diameter, 20 μm) connected to a flame ionized detector quantified the concentrations of combustible species and while a packed column (HayeSep Q, 2 m length, 2 mm inner diameter) connected to a thermal conductivity detector measured non-combustible products (i.e., H_2, H_2O, CO, and CO_2). Retention times and sensitivity factors of products were determined by injecting gaseous and liquid standards into the system. A complete list of these standards and calculations for sensitivity factors are shown in the Supplemental Information

(Section SI 3). Control of temperature, reactant flowrates, and the GC sampling were automated to allow for continuous measurements.

Ethanol conversions (X_{EtOH}) were calculated on a carbon basis,

$$X_{EtOH} = \frac{\sum_i P_i n_i}{\sum_i P_i n_i + 2 * P_{o,EtOH}} \qquad \text{Eq. S3}$$

where P_i and $P_{o,EtOH}$ represent the pressure at the outlet of product species, i, and C_2H_5OH, n_i is the carbon number of the each product, i. During selectivity measurements, X_{EtOH} is kept below 33.4% at which point C_2H_5OH, C_2H_4O, and H_2 pressures approach equilibrium concentrations for the hydrogenation and dehydrogenation of C_2H_4O and C_2H_5OH (Eq. S3) assuming the selectivity for dehydrogenation, $S_{dehydro}$, is 100%.

$$C_2H_5OH \rightleftarrows C_2H_4O + H_2 \qquad \text{Eq. S4}$$

Equilibrium concentrations were calculated using thermodynamic data,[9] where the approach to equilibrium factor (η) is equal to unity based on the following equation,

$$\eta = \frac{[C_2H_4O][H_2]}{[C_2H_5OH]e^{-\Delta G/RT}} \qquad \text{Eq. S5}$$

where R is the ideal gas constant, T is temperature (503 K), ΔG is the free energy of dehydrogenation, and $[C_2H_5OH]$, $[C_2H_4O]$, and $[H_2]$ are the partial pressure of ethanol, acetaldehyde, and hydrogen, respectively. When C_2H_5OH and C_2H_4O were co-fed, residence times were controlled to maintain differential conversion of each reactant (i.e., $X_a < 10\%$, X_a is the conversion for reactant a),

$$X_a = \frac{|P_{in,a} - P_{out,a}|}{P_{in,a}} \qquad \text{Eq. S6}$$

Where $P_{in,a}$ and $P_{out,a}$ are the inlet and outlet partial pressures, respectively, of reactant species a.

Products were separated into groups based on the possible reaction pathway (Scheme S1), and the selectivities for each product group were calculated as

$$S_k = \frac{\sum_j P_j n_j}{\sum_i P_i n_i} \qquad \text{Eq. S7}$$

where S_k is the selectivity of product group k, and P and n are the outlet pressure and carbon number, respectively, of all product species i and product species j formed in group k. Formation rates of product groups (e.g., dehydrogenation, esterification, and decarbonylation) were calculated based on the selectivity for product group,

$$r_k = \frac{\sum_j P_j \, n_j \quad (\dot{n}_{EtOH} + \dot{n}_{AA})}{2 * \sum_a P_{in,a} \quad n_{Cu,s}}$$

Eq. S8

where r_k is the formation rate of product group k, $\dot{n}_{EtOH}$ and $\dot{n}_{AA}$ are the molar flowrates of the C_2H_5OH and C_2H_4O, respectively, and $n_{Cu,s}$ is the moles of surface Cu atoms based on the measured dispersions (Table S4). Carbon balance closed within ± 5%.

Table S4. Catalyst synthesis conditions and cluster size

Catalyst	Synthesis Technique	Cluster Composition[a] (wt% Cu)	Oxidation Temperature[b] (K)	Reduction Temperature[c] (K)	d_{EXAFS}[d] (nm)	$<d_{TEM}>$[e] (nm)
2 nm Cu-SiO_2	IE	1.74	773	773	1.9	1.8 ± 0.8
8 nm Cu-SiO_2	IE	1.17	773	973	5.9	8 ± 3
29 nm Cu-C	IE	0.84	773	773	NT	30 ± 9
35 nm Cu-SiO_2	Sol-gel	1.67	773	573	-- [f]	35 ± 11
Cu-Al_2O_3	IW	10.3	773	573	NT	10 ± 3
Cu-ZnO	Coprecipitation	0.82 Cu : Zn	773	573	5.4	5 ± 2
Cu-ZnO-Al_xO_y	Coprecipitation	1.0 Cu : Zn 1.87 Cu : Al	773	573	5.1	6 ± 2
Cu-Al_xO_y	Coprecipitation	0.79 Cu : Al	773	573	3.4	5 ± 1
Cu-TiO_2	Sol-gel	0.41 Cu : Ti	773	573	7.8	12 ± 4
Cu-MgO	IW	3.33	773	573	--[g]	9 ± 3
Unsupported Cu	Decomposition	99.87[h]	773	573	-- [f]	NT
8 nm Cu-C	IW	1.41	773	973	6.5	8 ± 3
3 nm Cu-SiO_2	IE	1.85	923	773	2.2	3 ± 1
30 nm Cu-SiO_2	IW	1.80	773	573	NT	30 ± 12
Raney Cu	--	99.9996 ($4x10^4$ % Al)	N/A	573	4.5	NT
Cu- CrO_x	--	45.5	773	573	6.3	20 ± 8

[a] Metal content of samples determined by inductively coupled plasma optical emission spectroscopy (ICP-OES) following digestion in strong acid solutions. [b] 300 mL min^{-1} dry air [c] 25 kPa H_2 75 kPa He, 400 ml min^{-1} [d] Calculated from correlations derived by Miller *et al.*[8] [e] Surface area normalized average cluster diameter determined from > 100 clusters [f] Clusters larger than 10 nm is outside the range for EXAFS fitting [g] Dispersion could not be derived through EXAFS fitting due to interference from mixed oxide phase (i.e., CuMgO) in the Cu-Cu scattering. [h] Residual carbon measured by CHN analysis.

Table S5. Relative compositions of metals in coprecipitated and sol-gel catalysts measured through ICP-OES.

Catalyst	Cu (%)	Zn (%)	Al (%)	Ti (%)
Cu-ZnO	44	56	0	0
Cu-ZnO-Al_xO_y	35	44	21	0
Cu-Al_xO_y	44	0	56	0
Cu-TiO_2	29	0	0	71

Table S6. Fit of the Cu-K edge EXAFS for Cu foil and supported Cu catalysts at 298 K in 40% H_2/60% He after reduction treatment during TPR-XANES, 5 K min^{-1} to 773 K in 40% H_2/60% He

Sample	**Edge**	**Absorber-Backscatterer**	**N**	**R (Å)**	**$\Delta\sigma^2$ (Å^2)**	**ΔE_0 (eV)**	**Dispersion (%)**	**Particle size (nm)**
Cu Foil	Cu	Cu-Cu	12.0	2.54	--	--	Bulk	--
2 nm Cu-SiO_2	Cu	Cu-Cu	7.0	2.52	0.001	-1.2	47	1.9
8 nm Cu-SiO_2	Cu	Cu-Cu	10.7	2.54	0.001	0.7	16	5.9
35 nm SiO_2	Cu	Cu-Cu	12.0	2.54	0.001	0	Bulk	--
Cu-ZnO	Cu	Cu-Cu	10.4	2.57	0.001	-0.5	17	5.4
Cu-ZnO-Al_xO_y	Cu	Cu-Cu	10.2	2.54	0.001	0.7	18	5.1
Cu-Al_xO_y	Cu	Cu-Cu	8.9	2.55	0.001	-0.5	27	3.4
Cu-TiO_2	Cu	Cu-Cu	11.6	2.54	0.001	-0.7	12	7.8
8 nm Cu-C	Cu	Cu-Cu	11.0	2.54	0.001	0.5	14	6.5
3 nm Cu-SiO_2	Cu	Cu-Cu	7.3	2.52	0.001	-1.5	42	2.2
Raney Cu	Cu	Cu-Cu	9.8	2.54	0.001	0.3	20	4.5
Cu-CrO_x	Cu	Cu-Cu	10.9	2.54	0	0.4	14	6.3

Table S7. Fit of the Cu-K edge XANES at 573 K for supported Cu catalysts to using reference materials during TPR-XANES, 5 K min^{-1} in 40% H_2/60% He

Sample	**Linear Combination Fit**					**$Cu^{\delta+}$ / Cu^0**
	Bulk Cu^{2+}	**Small Cu^{2+}**	**Bulk Cu^{1+}**	**Small Cu^{1+}**	**Cu Foil**	
2 nm Cu-SiO_2	0	0	0.11	0.17	0.72	0.39
8 nm Cu-SiO_2	0	0	0.024	0.09	0.886	0.13
35 nm SiO_2	0	0	0.015	0.056	0.93	0.08
Cu-ZnO	0	0	0.018	0.039	0.943	0.06
Cu-ZnO-Al_xO_y	0	0	0.069	0.132	0.799	0.25
Cu-Al_xO_y	0	0	0.046	0.181	0.773	0.29
Cu-TiO_2	0	0	0	0.105	0.895	0.12
8 nm Cu-C	0	0	0.042	0.058	0.9	0.11
3 nm Cu-SiO_2	0	0	0.109	0.165	0.725	0.38
Raney Cu	0	0	0	0.12	0.88	0.14
Cu-CrO_x	0	0	0.027	0.07	0.903	0.11

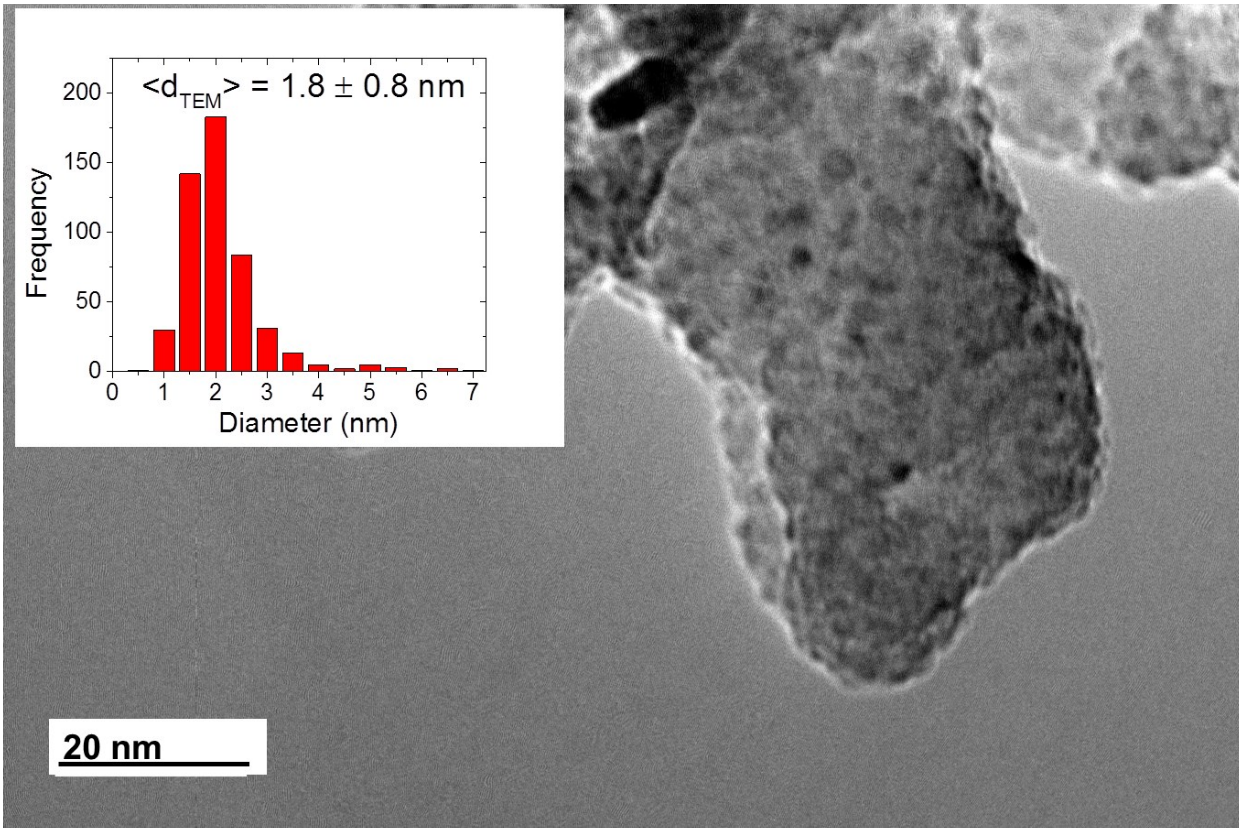

Figure S9. TEM image of 2 nm Cu-SiO_2 and cluster size distribution used to determine surface area normalized average cluster diameter, $\langle d_{TEM} \rangle$

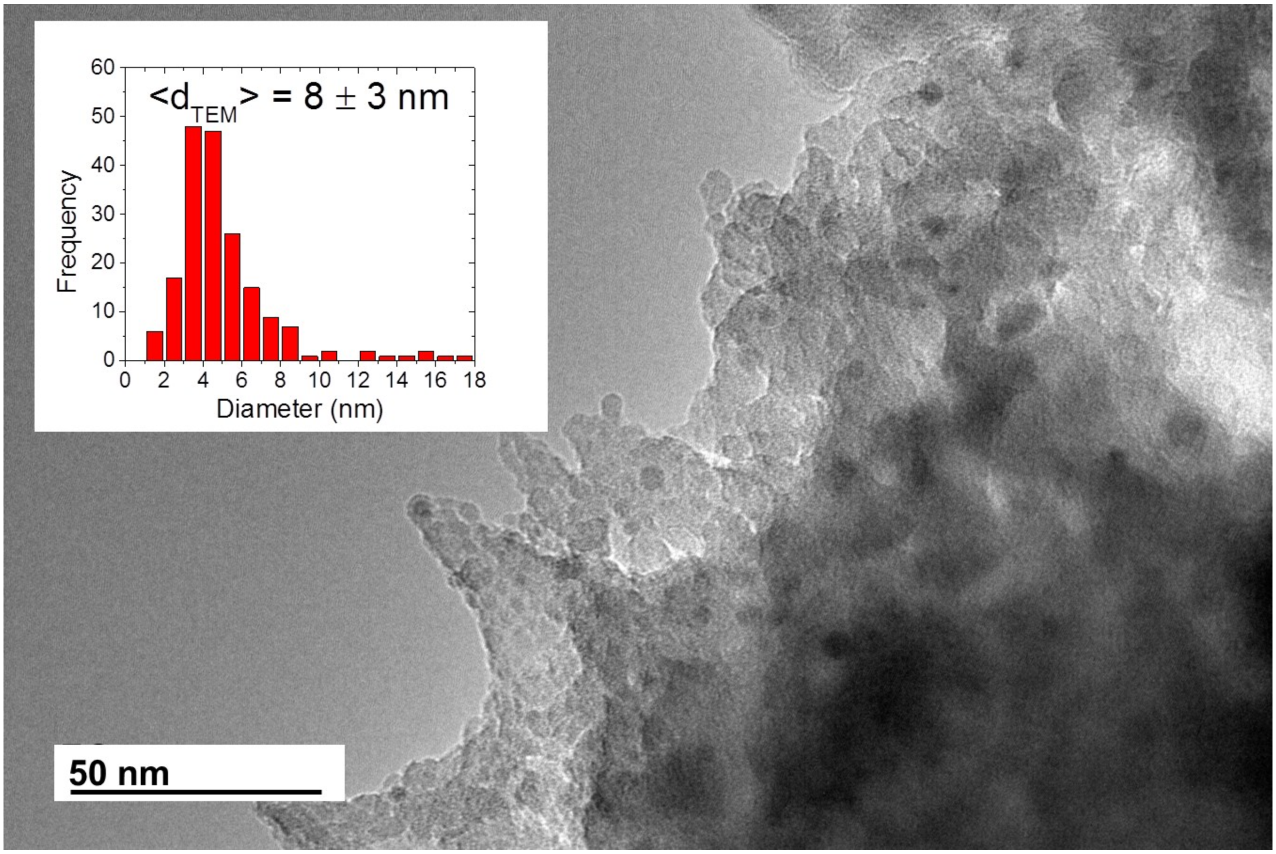

Figure S10. TEM image of 8 nm Cu-SiO_2 and cluster size distribution used to determine surface area normalized average cluster diameter, $<d_{TEM}>$

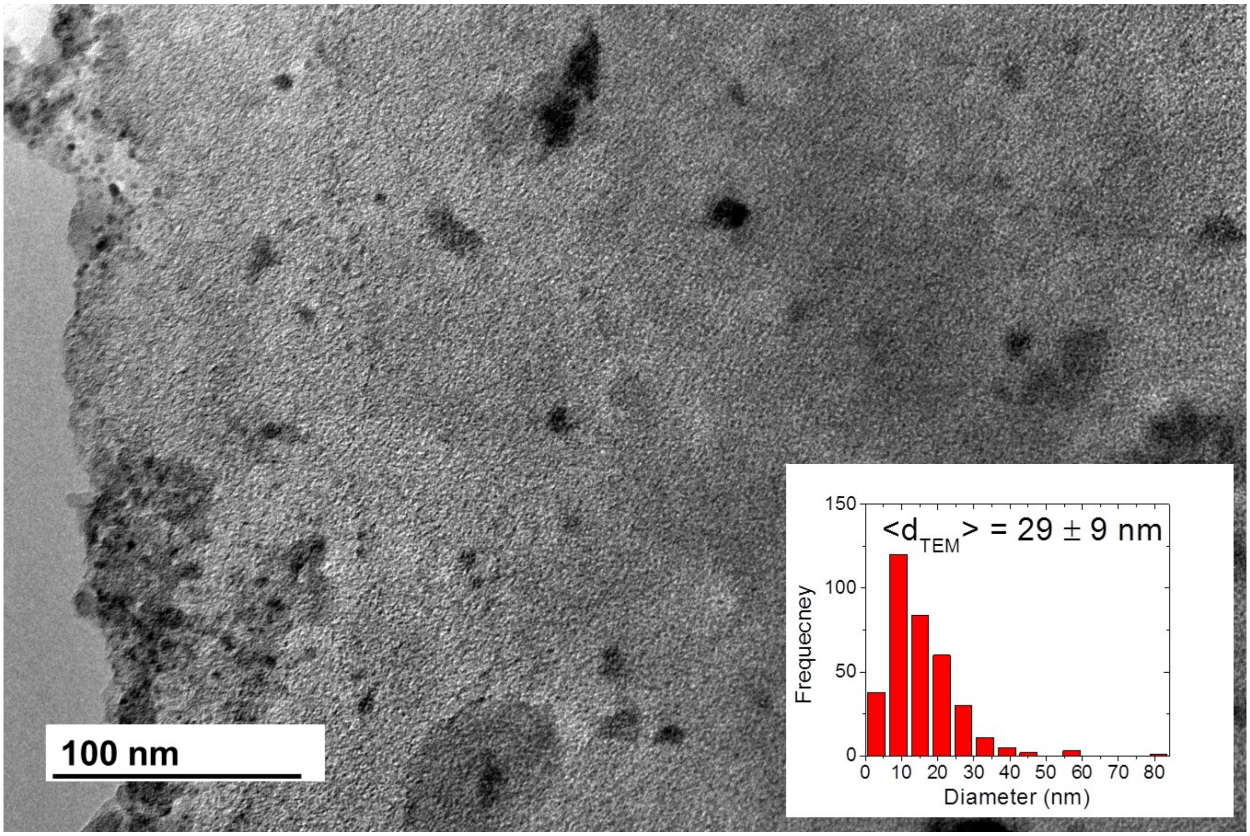

Figure S11. TEM image of 29 nm Cu-C and cluster size distribution used to determine surface area normalized average cluster diameter, <d_{TEM}>

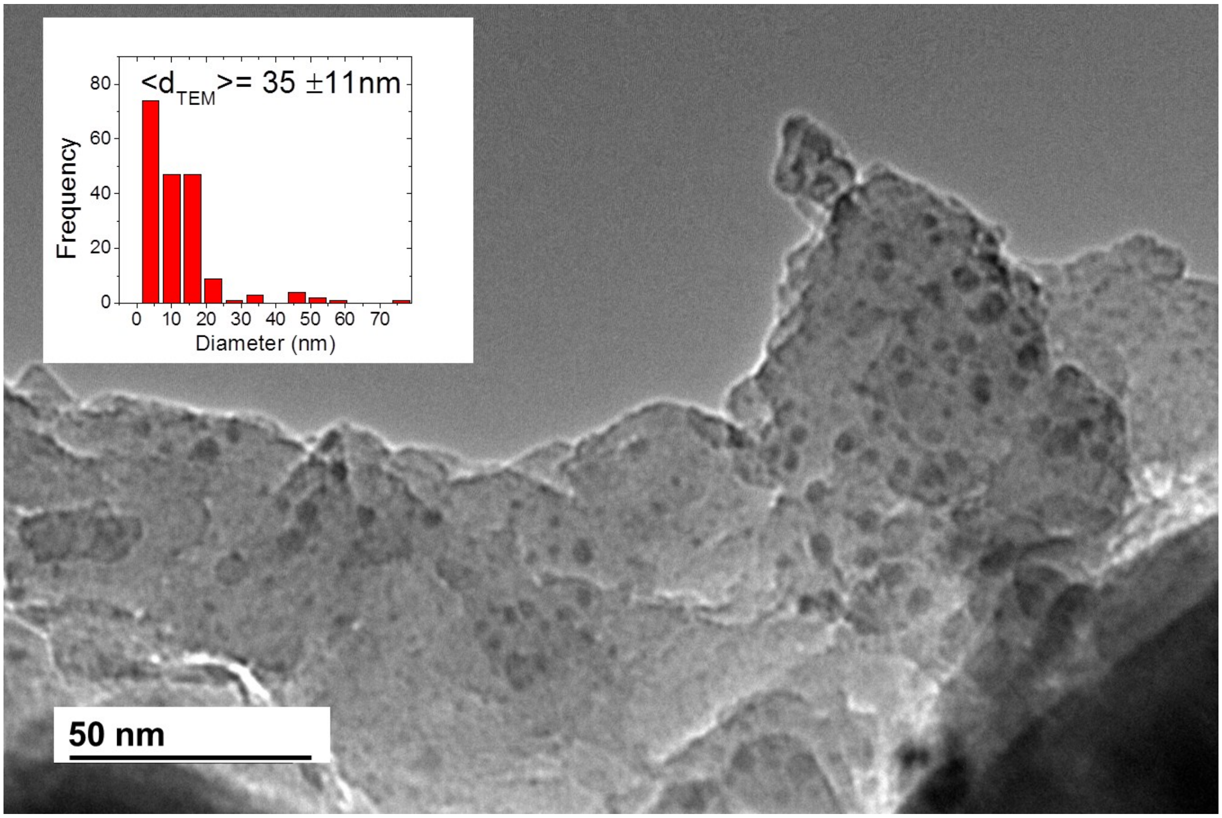

Figure S12. TEM image of 35 nm Cu-SiO_2 and cluster size distribution used to determine surface area normalized average cluster diameter, $<d_{TEM}>$

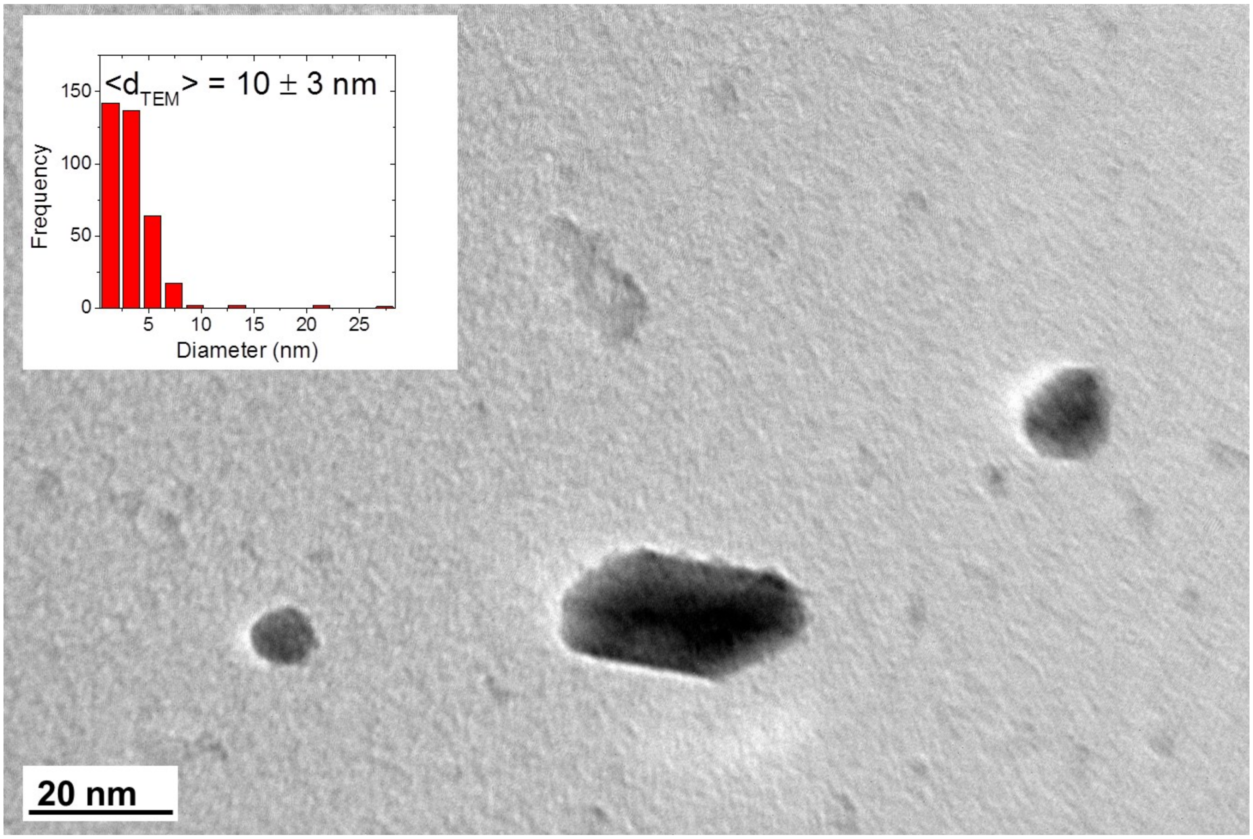

Figure S13. TEM image of Cu-Al_2O_3 and cluster size distribution used to determine surface area normalized average cluster diameter, $<d_{TEM}>$

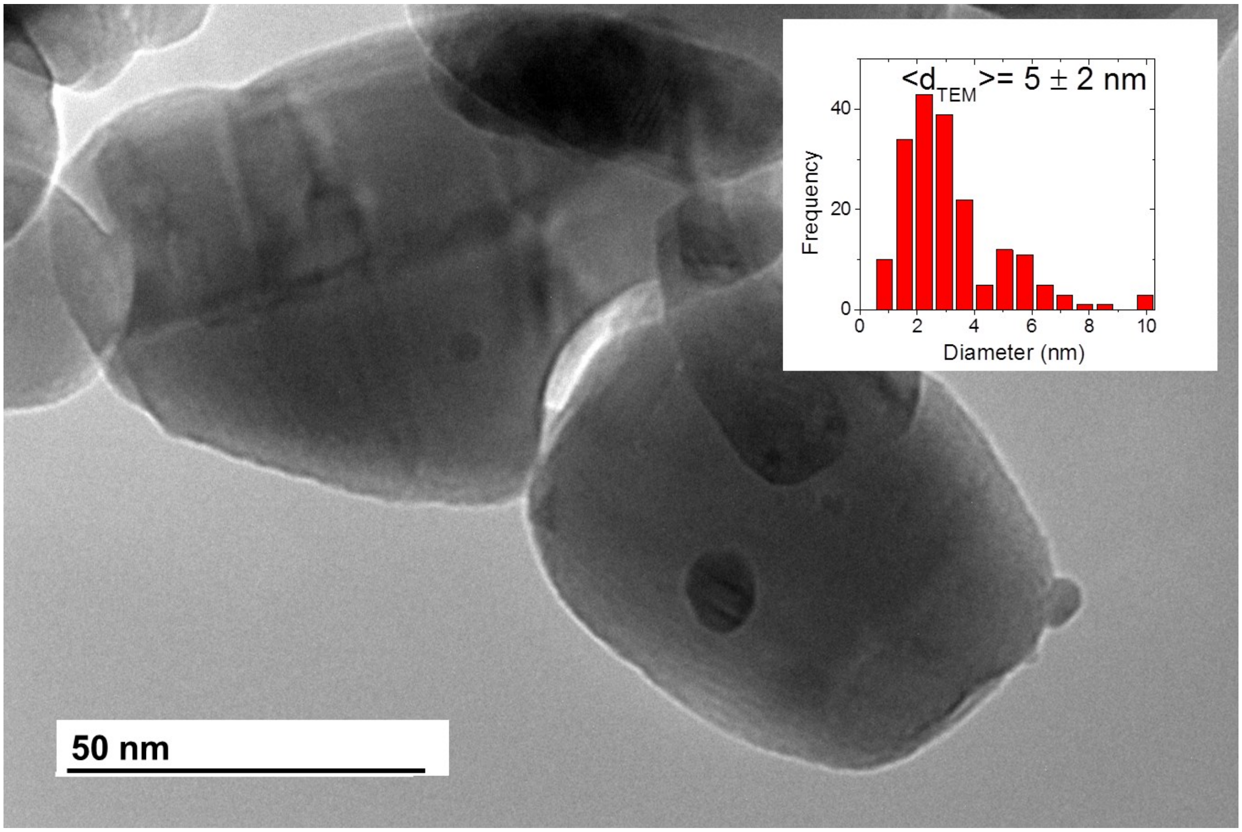

Figure S14. TEM image of Cu-ZnO and cluster size distribution used to determine surface area normalized average cluster diameter, $<d_{TEM}>$

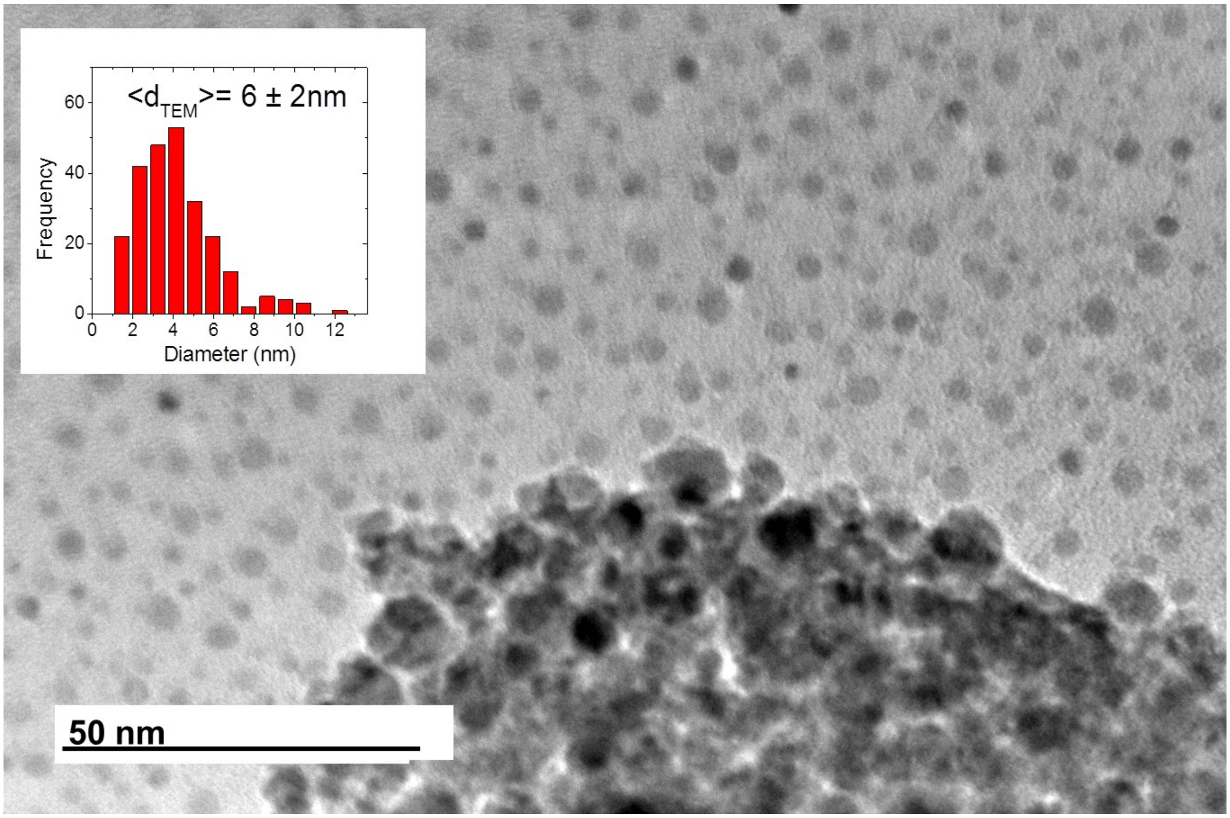

Figure S15. TEM image of Cu-ZnO-Al_xO_y and cluster size distribution used to determine surface area normalized average cluster diameter, $<d_{TEM}>$

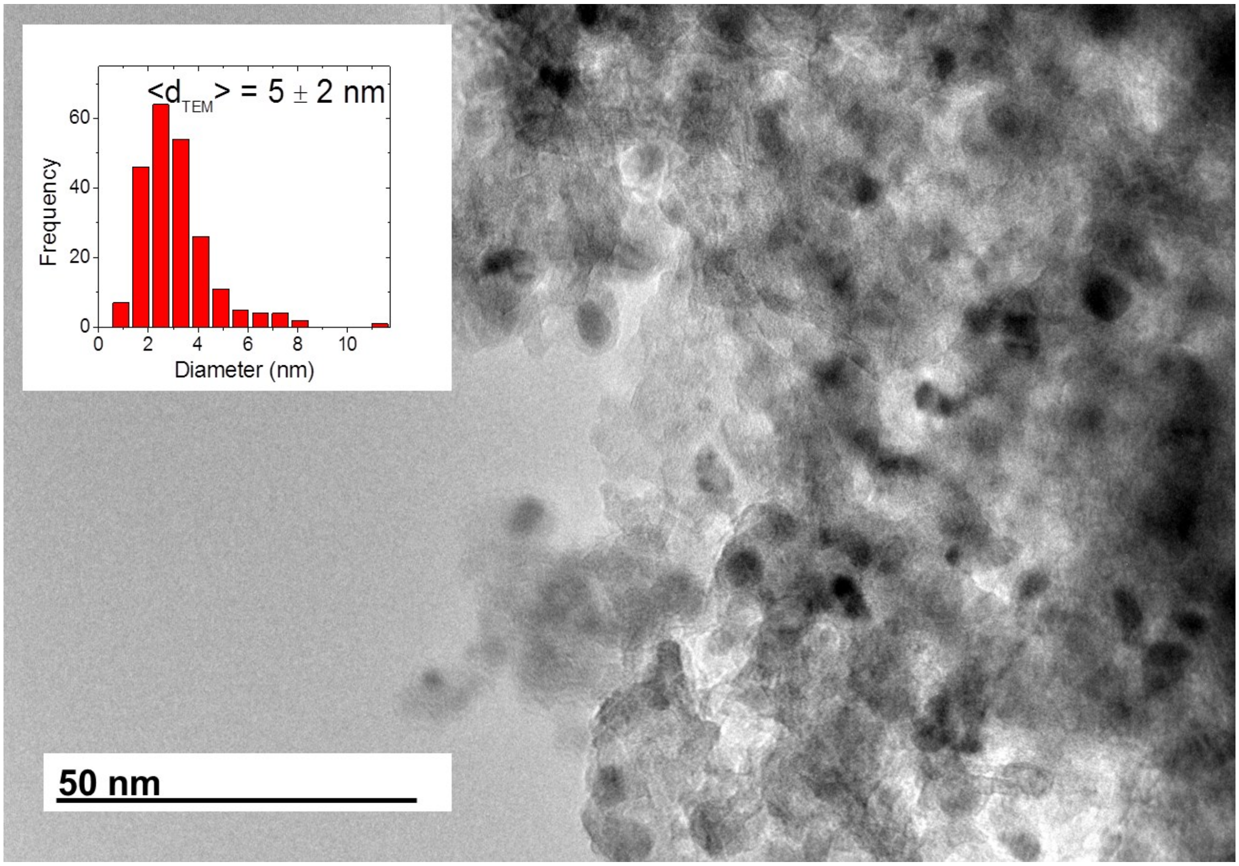

Figure S16. TEM image of Cu-Al_xO_y clusters and cluster size distribution used to determine surface area normalized average cluster diameter, $<d_{TEM}>$

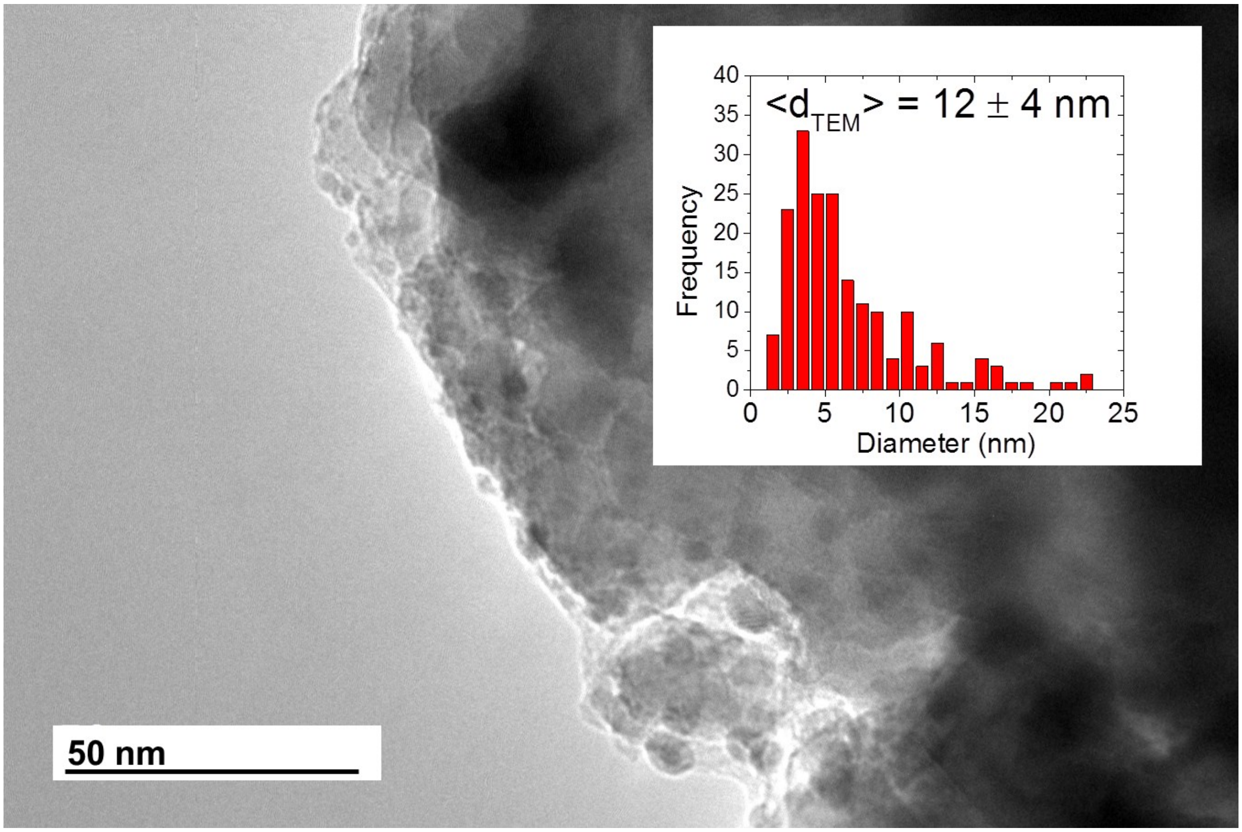

Figure S17. TEM image of Cu-TiO_2 clusters and cluster size distribution used to determine surface area normalized average cluster diameter, $\langle d_{TEM} \rangle$

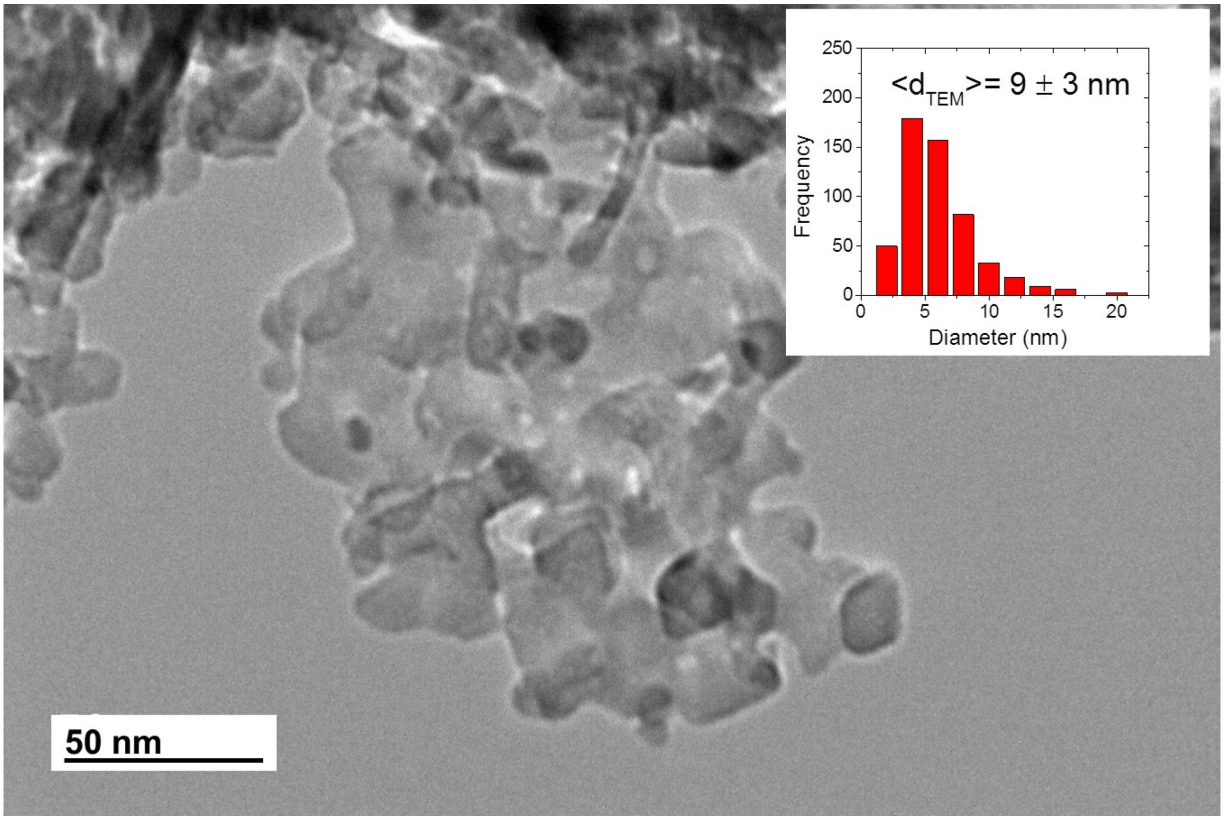

Figure S18. TEM image of Cu-MgO and cluster size distribution used to determine surface area normalized average cluster diameter, $\langle d_{TEM} \rangle$

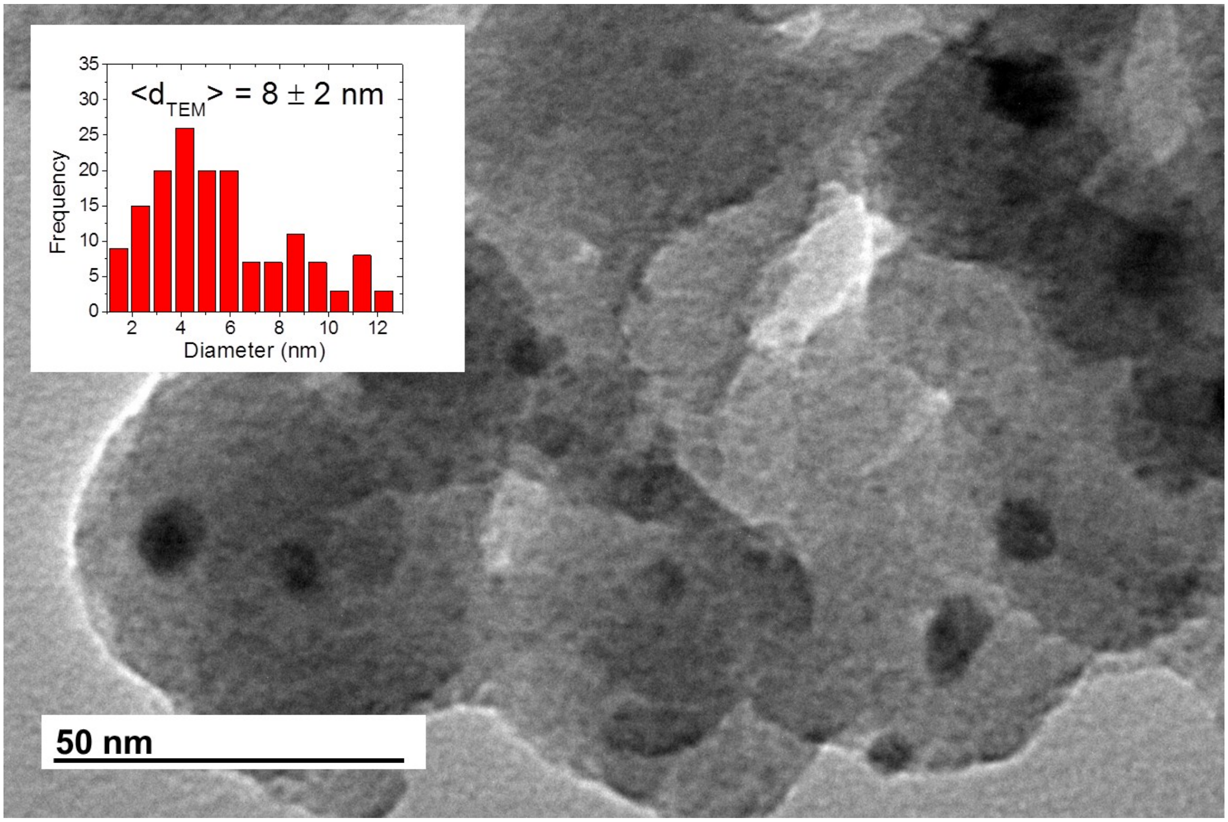

Figure S19. TEM image of 8 nm Cu-C and cluster size distribution used to determine surface area normalized average cluster diameter, $<d_{TEM}>$

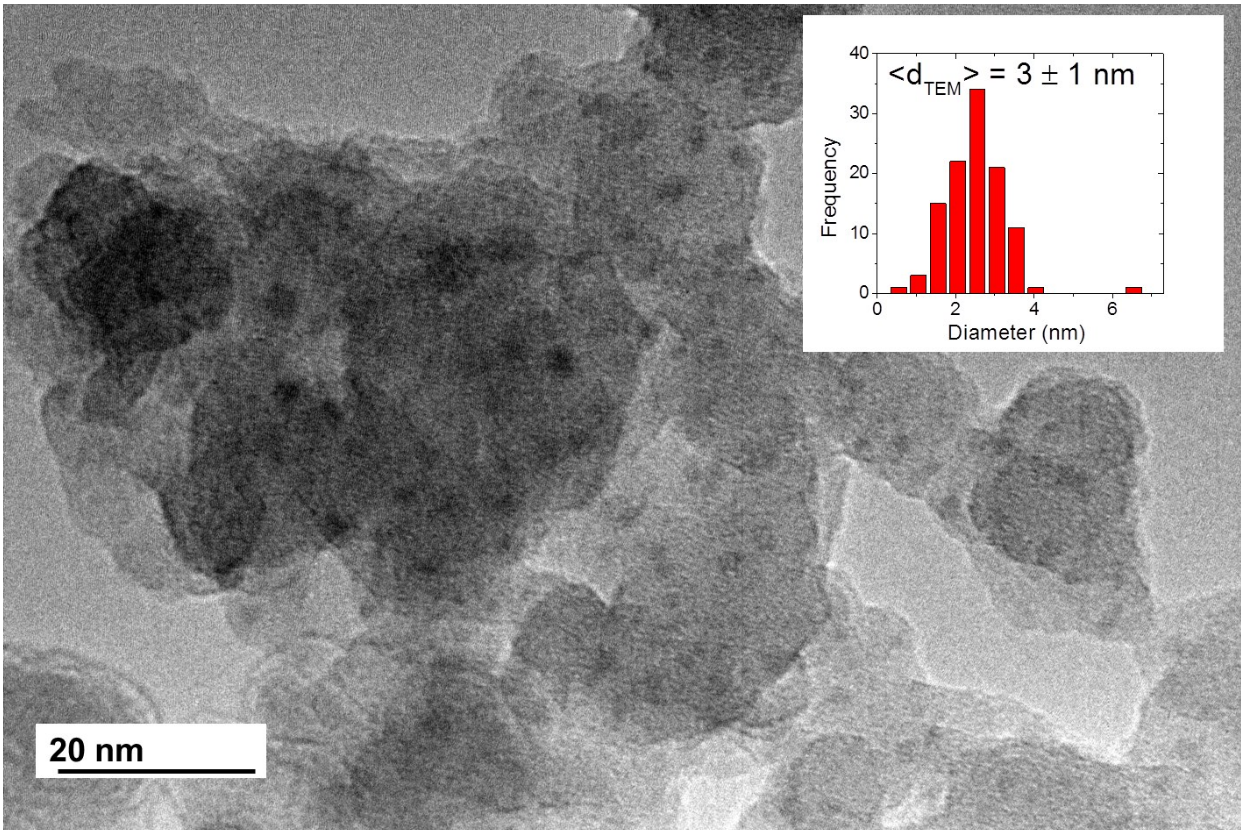

Figure S20. TEM image of 3 nm Cu-SiO_2 and cluster size distribution used to determine surface area normalized average cluster diameter, <d_{TEM}>

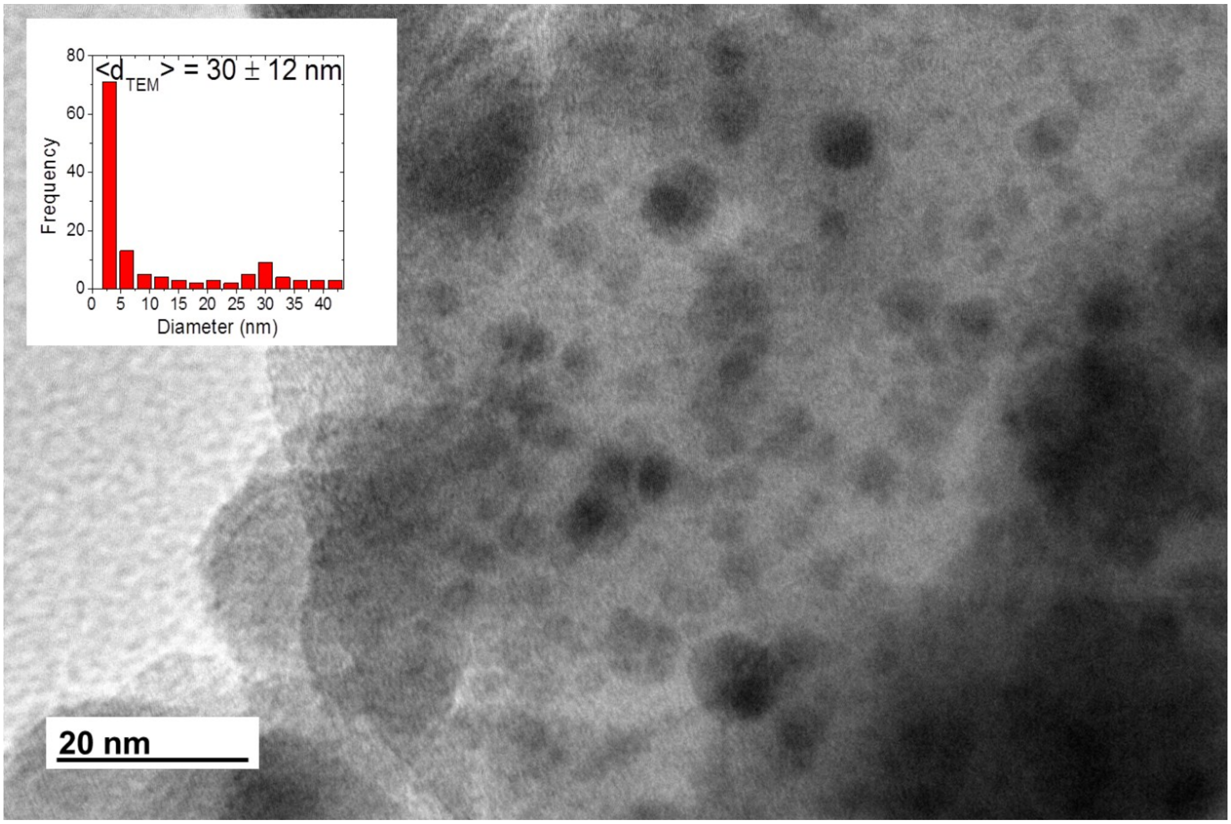

Figure S21. TEM image of 30 nm Cu-SiO_2 and cluster size distribution used to determine surface area normalized average cluster diameter, $\langle d_{TEM} \rangle$

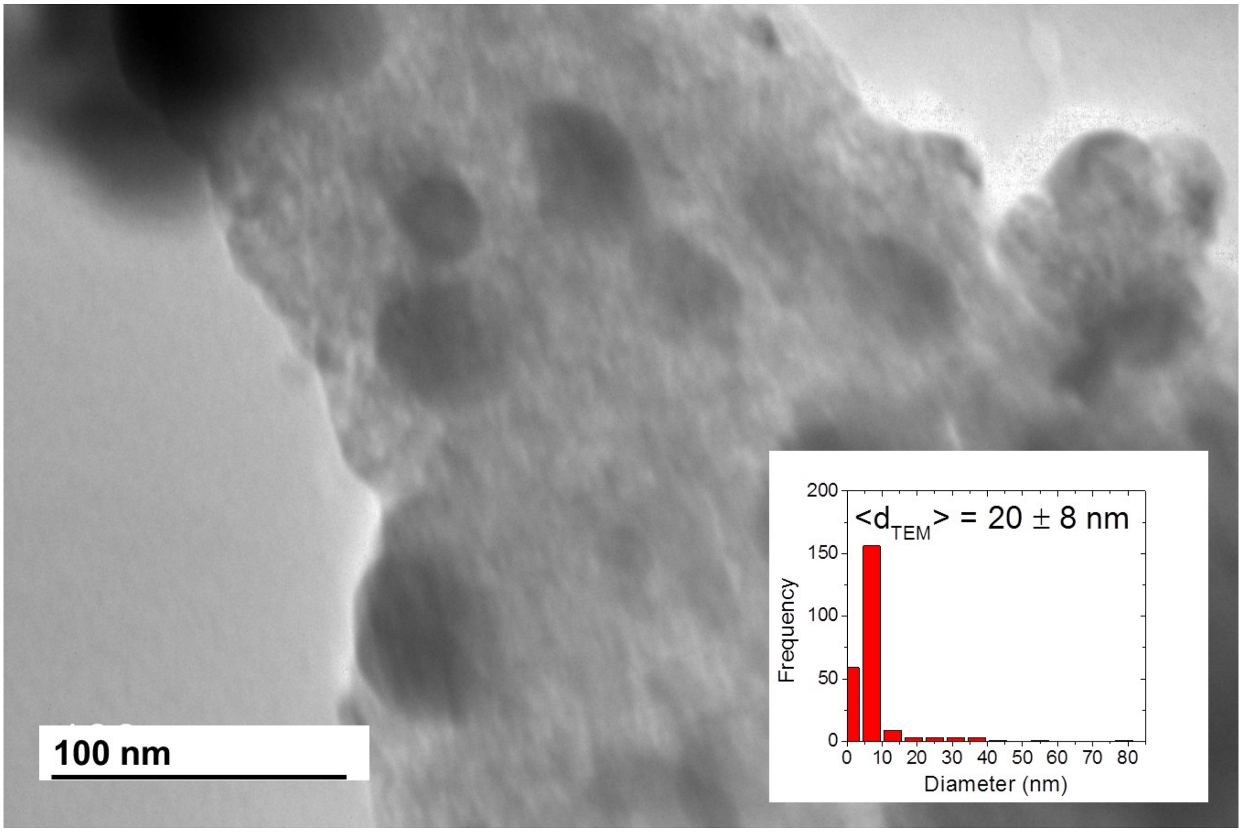

Figure S22. TEM image of Cu-CrO$_x$ and cluster size distribution used to determine surface area normalized average cluster diameter, <d$_{TEM}$>

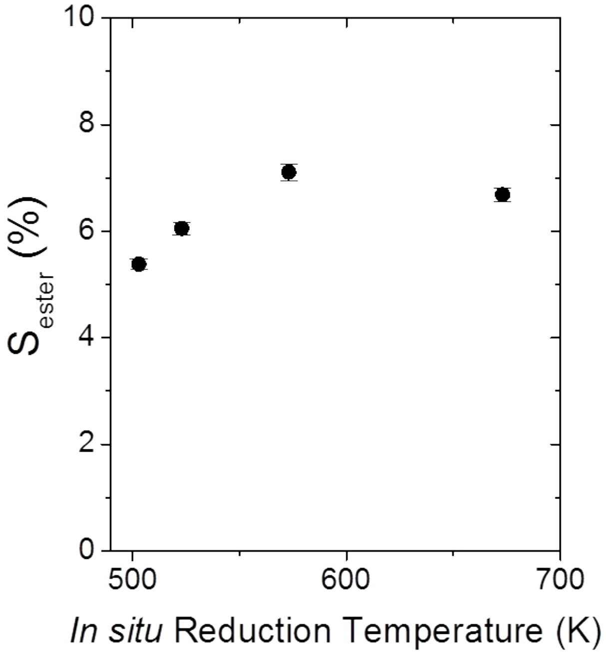

Figure S23. Selectivity for esterification at X_{EtOH} = 10% as a function of *in situ* reduction temperature over 6 nm Cu-CrO_x (2.75 kPa C_2H_5OH, 15 kPa H_2, 503 K).

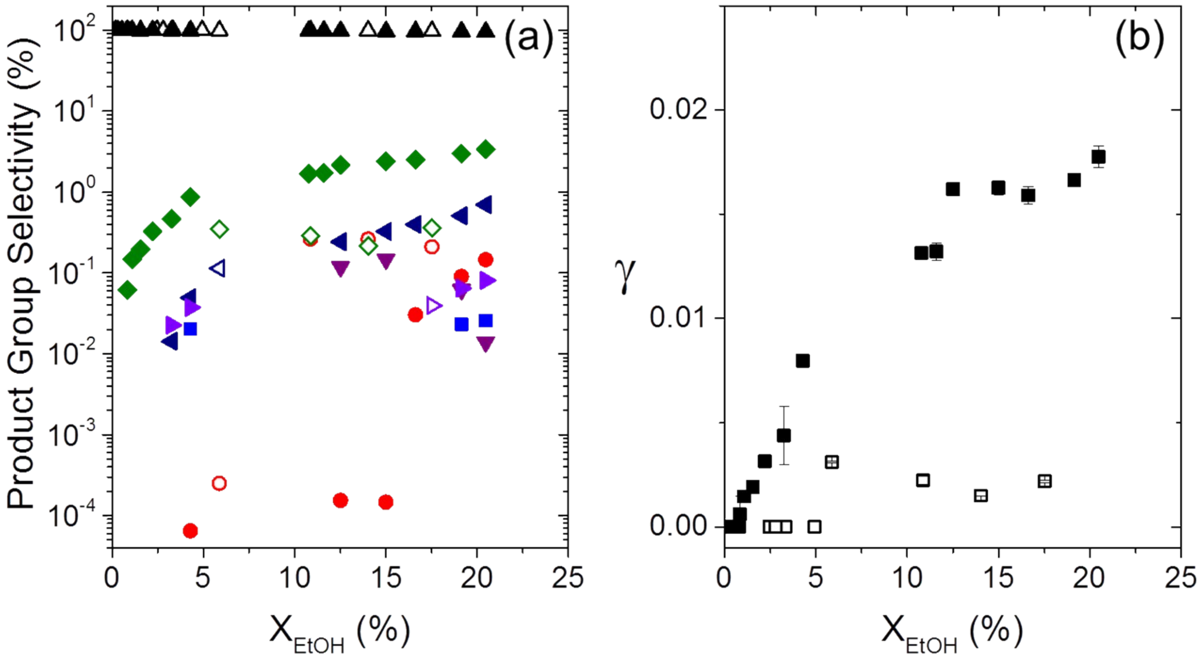

Figure S24. a) Changes in selectivity for dehydrogenation (▲), esterification (◆), ketonization (◀), decarbonylation (●), aldol addition (▶), etherification (▼), and dehydration (■); and b) ratio of esterification and dehydrogenation rates (γ) as functions of X_{EtOH} on 6 nm Cu-CrO_x (filled) and Cu-ZnO (hollow) (2.75 kPa C_2H_5OH, 15 kPa H_2, 503 K). γ values are calculated using dehydrogenation rates that have been adjusted for the approach to equilibrium to solely compare forward rates of reaction for esterification and dehydrogenation.

Conversion of ethanol is limited by the reverse reaction of acetaldehyde and H_2 to ethanol. The approach to equilibrium (η) is equal to unity at ~33.4% conversion of ethanol to acetaldehyde given a $\Delta G_{dehydrogenation}$ is 10.56 kJ mol^{-1} at 503 K based on tabulated values.[9,10] The ethanol conversion to reach equilibrium for dehydrogenation of ethanol and hydrogenation of acetaldehyde assumes 100% selectivity for acetaldehyde formation, which as Figure 1 indicates is not the case; however, at ethanol conversions greater than 33.4%, selectivity for acetaldehyde would decrease and the selectivity for the other reactions (e.g., decarbonylation, esterification, aldol addition) would increase by slowly consuming the equilibrated pool of ethanol and acetaldehyde.

SI 3. Standards and Calibrated Sensitivity Factors for Gas Chromatograph

In all the experiments, ethanol was used as a standard to calibrate the pressures of the liquid reactants and products. Initially, a measured amount of ethanol was injected through the system by-pass and the gas chromatograph gas sampling valve. The sensitivity factor of ethanol, F_{EtOH}, was calculated by taking the ratio of the known pressure of the ethanol to the peak area as shown in the following equation,

$$F_{EtOH} = \frac{P_{EtOH}}{A_{EtOH}} \qquad \text{Eq. S9}$$

where P_{EtOH} and A_{EtOH} are the pressure and measured peak area of ethanol, respectively. Sensitivity factors of other components were calculated by injecting known ratios of ethanol to other desired components directly to the capillary column of the GC. Since the mole ratio is proportional to the peak areas, the sensitivity factor of different components, F_i, were calculated using the following equation,

$$\frac{F_{EtOH} * A_{EtOH}}{F_i * A_i} = \frac{N_{EtOH}}{N_i} \qquad \text{Eq. S10}$$

Where A_i is the measured peak area and $\frac{N_{EtOH}}{N_i}$ is the mole ratio of ethanol to species *i*.

Consequently the pressures of the desired products were calculated utilizing the sensitivity factor derived above as shown in the following equation

$$P_i = P_{EtOH} * F_i * \frac{A_i}{A_{EtOH}} \qquad \text{Eq. S11}$$

Here, P_i is the pressure of species *i* in the effluent stream.

Gas species were calibrated by introducing a multi-component gas mixture into the GC through the gas sampling valve. Sensitivity factors were calculated by dividing the pressure by the peak area observed, using the equation

$$F_i = \frac{P_i}{A_i} \qquad \text{Eq. S12}$$

The pressure of each species *i*, P_i, of the gases were calculated assuming the validity of the ideal gas law. Consequently, the pressures of the products were quantified by multiplying the sensitivity factor that was derived above by the peak area:

$$P_i = F_i * A_i \qquad \text{Eq. S13}$$

The following chemicals were used as standards for the calibration of sensitivity factors and retention times:

- Ethanol, Decon Laboratory, 200 proof
- Acetaldehyde, Fluka Analytical, ≥99.5%
- 1-butanol, Fisher Scientific, 99.9%
- Butyraldehdye (Fluka, 99%)

- Diethyl ether, Fisher Scientific, 99.9%
- Acetone, Macron Fine Chemicals, ACS grade
- Pyridine, Fisher chemicals, 99.9%
- Octanol, Aalfa Aesar, 99%
- Croton Aldehyde, Aldrich Chemistry, 99%
- Crotyl Alcohol, Aldrich Chemistry, 96%
- Butyl acetate, Fulka Analytical
- 1-Hexanol, sigma Aldrich, 98%
- 2-ethyl butanol, Sigma Aldrich, 98%
- Hexanal, Aldrich chemistry, 98%
- Ethyl acetate, Macron Fine Chemicals, ACS grade
- 2-ethyl hexanol, Sigma Aldrich, 96%
- Iso-propanol, Macron Fine Chemicals, ACS grade
- Octanol, Alfa Aesar, 99%
- Butyric acid, Aldrich chemistry, 99.9%
- Acetic acid, Fisher chemicals, 99.7%
- Butanal, Fluka Analytical, ≥99%
- MEK, Sigma Aldrich, ACS reagent, ≥99%

The two separate multi-component gas mixtures were used to calibrate the gaseous species:

- Scotty Analyzed Gases, 15.5 ppm acetylene, 15.2 ppm n-butane, 15.2 ppm ethane, 15.1 ppm ethylene, 15.2 ppm methane, 15.1 ppm propane, 15.2 ppm propylene, 15.3 ppm methyl acetylene bal. nitrogen
- Scotty Analyzed Gases 1.01% acetylene, 1.0% carbon dioxide, 1.0% carbon monoxide, 1.01% ethane, 1.01% ethylene, 1.01% methane bal. nitrogen

Gas mixtures where injected through the GSV to determine retention time and sensitivity factors.

References

1. C. P. Jimenez-Gomez, J. A. Cecilia, D. Duran-Martin, R. Moreno-Tost, J. Santamaria-Gonzalez, J. Merida-Robles, R. Mariscal and P. Maireles-Torres, *J. Catal.*, 2016, **336**, 107-115.
2. Y. H. Zhao, Z. Horita, T. G. Langdon and Y. T. Zhu, *Mat. Sci. Eng., A*, 2008, **474**, 342-347.
3. T. Kasai, X. Y. Fu, D. A. Rigney and A. L. Zharin, *Wear*, 1999, **225**, 1186-1204.
4. J. Zhang, M. J. Li, Z. C. Feng, J. Chen and C. Li, *J. Phys. Chem. B*, 2006, **110**, 927-935.
5. L. Jiao and J. R. Regalbuto, *J. Catal.*, 2008, **260**, 329-341.
6. E. Geravand, Z. Shariatinia, F. Yaripour and S. Sahebdelfar, *Chem. Eng. Res. Des.*, 2015, **96**, 63-77.
7. B. Ravel and M. Newville, *J. Synchrotron Radiat.*, 2005, **12**, 537-541.
8. J. T. Miller, A. J. Kropf, Y. Zha, J. R. Regalbuto, L. Delannoy, C. Louis, E. Bus and J. A. van Bokhoven, *J. Catal.*, 2006, **240**, 222-234.
9. C. L. Yaws, *Yaws' handbook of thermodynamic and physical properties of chemical compounds physical, thermodynamic and transport properties for 5,000 organic chemical compounds*, 2003, 1 online resource.
10. D.R. Burgess, “Thermochemical Data,” *NIST Chemistry WebBook, NIST Standard Reference Database Number 69*, 2016, **20899**, http://webbook.nist.gov.